

# The Effect of Greenhouse Gas–Induced Changes in SST on the Annual Cycle of Zonal Mean Tropical Precipitation

JOHN G. DWYER

*Department of Applied Physics and Applied Mathematics, Columbia University, New York, New York*

MICHELA BIASUTTI

*Lamont-Doherty Earth Observatory, Columbia University, Palisades, New York*

ADAM H. SOBEL

*Department of Applied Physics and Applied Mathematics, Department of Earth and Environmental Sciences, and Lamont-Doherty Earth Observatory, Columbia University, New York, New York*

(Manuscript received 9 April 2013, in final form 27 February 2014)

## ABSTRACT

Models from phase 5 of the Coupled Model Intercomparison Project (CMIP5) project changes to the seasonality of both tropical sea surface temperature (SST) and precipitation when forced by an increase in greenhouse gases. Nearly all models project an amplification and a phase delay of the annual cycle for both quantities, indicating a greater annual range and extrema reached later in the year. The authors investigate the nature of the seasonal precipitation changes in AGCM experiments forced by SST perturbations, which represent idealizations of the changes in annual mean, amplitude, and phase as simulated by CMIP5 models. A uniform SST warming is sufficient to force both amplification and a delay of the annual cycle of precipitation. The amplification is due to an increase in the annual mean vertical water vapor gradient, while the delay is affected by changes in the seasonality of the circulation. A budget analysis of this simulation reveals a large degree of similarity with the CMIP5 results. In the second experiment, only the seasonal characteristics of SST are changed. In response to an amplified annual cycle of SST, the annual cycle of precipitation is amplified, while for a delayed SST, the annual cycle of precipitation is delayed. Assuming that SST changes can entirely explain the seasonal precipitation changes, the AGCM simulations herein suggest that the annual mean warming explains most of the amplitude increase and much of the phase delay in the CMIP5 models. However, imperfect agreement between the changes in the SST-forced AGCM simulations and the CMIP5 coupled simulations suggests that coupled effects may play a significant role.

## 1. Introduction

The annual cycle of tropical precipitation, primarily characterized by the monsoons and the meridional movement of the ITCZ, is responsible for much of the variance in global precipitation. Even relatively small changes in the annual cycle of tropical precipitation may have large impacts, both globally and locally. For example, they can affect the timing and quantity of latent heat release and energy transport, which can also affect

the general circulation. Changes in monsoonal timing have large regional implications due to the dependence of many agricultural and pastoral communities on rainfall.

Nearly all of the models in the World Climate Research Programme's (WCRP's) Coupled Model Intercomparison Project phase 3 (CMIP3) multimodel dataset (Meehl et al. 2007) project consistent changes to the annual cycle of tropical SST and precipitation in simulations with increased greenhouse gases: a phase delay and an amplification (Chou et al. 2007; Tan et al. 2008; Biasutti and Sobel 2009; Sobel and Camargo 2011; Seth et al. 2011; Dwyer et al. 2012). Models from phase 5 of CMIP (CMIP5; Taylor et al. 2012) show changes of the same sign, as we discuss in section 3 and as documented elsewhere (Biasutti 2013; Seth et al. 2013; Huang et al. 2013).

---

*Corresponding author address:* John G. Dwyer, Department of Applied Physics and Applied Mathematics, Columbia University, 500 W. 120th St., New York, NY 10027.  
E-mail: jgd2102@columbia.edu

These CMIP3 and CMIP5 studies suggest a variety of causes to explain the projected changes in the annual cycle, including high-latitude phase delays due to reduced sea ice affecting the tropics; changes in the strength and extent of the Hadley cell affecting the amplitude of precipitation and SST via changes in the surface wind speed on turbulent surface fluxes; an increase in low-level water vapor vertically advected by the Hadley cell leading to an increase in the amplitude of precipitation; changes in the timing and strength of the annual cycle of surface heat fluxes affecting the annual cycle of surface temperature; increased vertical stability later in the year due to enhanced warming aloft delaying the timing of tropical precipitation; and a reduction of soil moisture early in the year in monsoon regions delaying monsoonal precipitation. Most of this work focuses on the projected amplitude changes, especially for precipitation. Projected phase changes have received less attention and are not as well understood.

We are interested in what modifies the annual cycles of both precipitation and surface temperature in the greenhouse gas–forced, fully coupled models. In this paper we address a more limited question: given a change in the annual mean or annual cycle of SST, what is the response of the annual cycle of precipitation and to what extent can this explain changes in the coupled models? Using an atmospheric general circulation model (AGCM) forced with SST provides a simple framework to evaluate this question, but there are drawbacks to this approach. In particular, prescribing SST eliminates feedbacks between the ocean and atmosphere that are present in both the real climate and coupled models (Fu and Wang 2004; Kitoh and Arakawa 1999). Despite this, given the observed SST and radiative forcings, AGCMs capture the annual precipitation anomalies over land and for the tropics overall, although there is some discrepancy over ocean (Liu et al. 2012). Similar studies where the annual cycle of SST was modified or suppressed have been carried out to study the effect of SST on the Asian summer monsoon (Shukla and Fennessy 1994), the equatorial Atlantic and Pacific (Li and Philander 1997), precipitation in the Amazon basin (Fu et al. 2001), and precipitation in the tropical Atlantic (Biasutti et al. 2003, 2004).

As we will show later, the AGCM experiments reproduce many aspects of the change in seasonality seen in the coupled models. This suggests to us that the same mechanism might be operating in the greenhouse gas–forced coupled models. (Here we use the term “seasonality” to denote the annual cycle only and not higher-frequency harmonics). While this study cannot rule out alternative mechanisms for the seasonality changes of precipitation in the coupled models, it demonstrates that changes to the annual mean and annual

cycle of SST are each sufficient to affect the annual cycle of precipitation simulated in the coupled models.

Ultimately, greenhouse gases are responsible for the changes to both SST and precipitation in the coupled models. While our results suggest that precipitation is responding to changes to SST, the mechanism by which greenhouse gases affect the seasonality of SST is not yet clear. Earlier research has suggested a link to the surface fluxes (specifically latent heat flux), which may be due to changes in the Hadley circulation (Sobel and Camargo 2011; Dwyer et al. 2012).

In the following section we describe the methods, AGCM, experimental design, and sensitivity of the results to our methods. Next in section 3 we describe the annual mean and seasonal changes to SST and precipitation in the CMIP5 models, which motivates the modeling studies. In sections 4 and 5 we describe and interpret the results of our simulations in which we uniformly increased the SST and changed the seasonality of SST, respectively. In section 6 we discuss how to interpret the coupled results in light of the uncoupled, idealized simulations. We conclude in section 7 and summarize our results.

## 2. Methods and experimental design

We reproduce the CMIP3 results of an amplitude increase and a phase delay for SST and precipitation in the tropics (25°S–25°N) with 35 CMIP5 models for which monthly precipitation and surface temperature data for both the historical simulation and representative concentration pathway 8.5 (RCP8.5) scenario are available. RCP8.5 is a high greenhouse gas emission scenario with a year 2100 radiative forcing of around  $8.5 \text{ W m}^{-2}$  relative to preindustrial conditions (Taylor et al. 2012). A full list of models included in this study is given in Table 1.

For our simulations, we use the atmospheric component [Community Atmosphere Model version 4 (CAM4)] of the National Center for Atmospheric Research (NCAR) Community Climate System Model, version 4 (CCSM4) (Gent et al. 2011) at the standard resolution ( $1.9^\circ \times 2.5^\circ$ ). To create a control simulation, we run the model for 40 years with climatological SST determined from the Hadley Center and the National Oceanic and Atmospheric Administration (NOAA) for the 1982–2001 observation period (Hurrell et al. 2008). The perturbed simulations were run for at least 10 years, sufficiently long to characterize the annual cycle of precipitation. The only change we made in the perturbed simulations was to alter either the mean or the annual cycle of SST. Land temperatures were free to adjust on their own and the atmospheric chemical composition was the same between simulations.

TABLE 1. The 35 CMIP5 models used in this study.

Model	Expansion, group, country
ACCESS1.3	Australian Community Climate and Earth-System Simulator, version 1.3, Commonwealth Scientific and Industrial Research Organisation (CSIRO) and Bureau of Meteorology (BoM), Australia
BCC-CSM1.1	Beijing Climate Center (BCC) Climate System Model, version 1.1, BCC, China
BCC-CSM1.1-m	BCC Climate System Model with moderate resolution, BCC, China
BNU-ESM	Beijing Normal University–Earth System Model, College of Global Change and Earth System Science (GCESS), China
CanESM2	Second Generation Canadian Earth System Model, Canadian Centre for Climate Modelling and Analysis (CCCma), Canada
CCSM4	Community Climate System Model, version 4, National Center for Atmospheric Research (NCAR) United States
CESM1-BGC	Community Earth System Model, version 1 (CESM1)–Biogeochemical, National Science Foundation (NSF)–Department of Energy (DOE)–NCAR, United States
CESM1-CAM5	CESM1 (Community Atmosphere Model, version 5) NSF–DOE–NCAR, United States
CESM1-WACCM	CESM1 (Whole Atmosphere Community Climate Model), NSF–DOE–NCAR, United States
CMCC-CM	Centro Euro-Mediterraneo sui Cambiamenti Climatici (CMCC) Climate Model, CMCC, Italy
CMCC-CMS	CMCC Climate Model with a resolved stratosphere, CMCC, Italy
CNRM-CM5	Centre National de Recherches Météorologiques (CNRM) Coupled Global Climate Model, version 5, CNRM–Centre Européen de Recherche et de Formation Avancée en Calcul Scientifique (CERFACS), France
CSIRO-Mk3.6.0	Commonwealth Scientific and Industrial Research Organisation (CSIRO) Mark, version 3.6.0, CSIRO–Queensland Climate Change Centre of Excellence (QCCCE), Australia
FGOALS-g2	Flexible Global Ocean–Atmosphere–Land System Model (FGOALS) gridpoint, version 2, State Key Laboratory of Numerical Modeling for Atmospheric Sciences and Geophysical Fluid Dynamics (LASG)–Center for Earth System Science, Tsinghua University (CESS), China
FGOALS-s2	FGOALS gridpoint, second spectral version, LASG–Institute of Atmospheric Physics (IAP), China
FIO-ESM	First Institute of Oceanography (FIO) Earth System Model, FIO, China
GFDL-CM3	Geophysical Fluid Dynamics Laboratory (GFDL) Climate Model, version 3, National Oceanic and Atmospheric Administration (NOAA) GFDL, United States
GFDL-ESM2G	GFDL Earth System Model with Generalized Ocean Layer Dynamics (GOLD) component, NOAA GFDL, United States
GFDL-ESM2M	GFDL Earth System Model with Modular Ocean Model 4 (MOM4) component, NOAA GFDL, United States
GISS-E2-R	Goddard Institute for Space Studies (GISS) Model E, coupled with the Russell ocean model National Aeronautics and Space Administration (NASA) GISS, United States
GISS-E2H	GISS Model E, coupled with the HYCOM ocean model, NASA GISS, United States
HadGEM2-CC	Hadley Centre Global Environment Model, version 2–Carbon Cycle, Met Office Hadley Centre (MOHC), United Kingdom
HadGEM2-ES	Hadley Centre Global Environment Model, version 2–Earth System, MOHC, United Kingdom
INM-CM4.0	Institute of Numerical Mathematics (INM) Coupled Model, version 4.0, INM, Russia
IPSL-CM5A-LR	L’Institut Pierre-Simon Laplace (IPSL) Coupled Model, version 5, coupled with NEMO, low resolution, IPSL, France
IPSL-CM5A-MR	IPSL Coupled Model, version 5, coupled with NEMO, mid resolution, IPSL, France
IPSL-CM5B-LR	IPSL, with Laboratoire de Météorologie Dynamique general circulation model, version 5B (LMDZ5B), atmospheric parameterization, IPSL, France
MIROC-ESM	Model for Interdisciplinary Research on Climate (MIROC), Earth System Model, Japan Agency for Marine–Earth Science and Technology (JAMSTEC), Atmosphere and Ocean Research Institute (AORI), The University of Tokyo, and National Institute for Environmental Studies (NIES), Japan
MIROC-ESM-CHEM	MIROC, Earth System Model, Chemistry Coupled, JAMSTEC–AORI–NIES, Japan
MIROC5	MIROC version 5, JAMSTEC–AORI–NIES, Japan
MPI-ESM-LR	Max Planck Institute (MPI) Earth System Model, low resolution, MPI for Meteorology (MPI-M), Germany
MPI-ESM-MR	MPI Earth System Model, low resolution, MPI-M, Germany
MRI-CGCM3	Meteorological Research Institute (MRI) Coupled Atmosphere–Ocean General Circulation Model, version 3, MRI, Japan
NorESM1-M	Norwegian Earth System Model, version 1 (intermediate resolution) (NorESM1-M), Norwegian Climate Centre (NCC), Norway
NorESM1-ME	NorESM1-M with carbon cycle, NCC, Norway

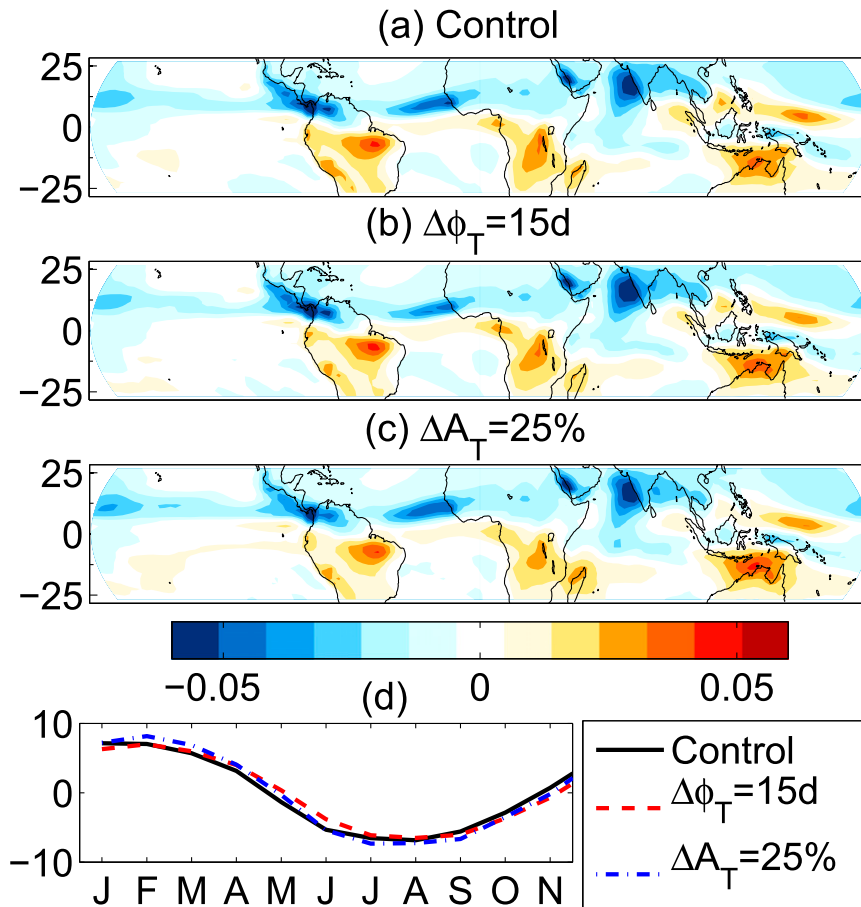


FIG. 1. The first EOF of tropical precipitation representing the annual cycle for (a) the control simulation, (b) a simulation forced with a 15-day phase delay of SST, and (c) a simulation forced with a 25% amplitude increase of SST. (d) The PC1s associated with each EOF.

We use two methods to calculate the seasonal characteristics of temperature and precipitation. The first is to Fourier transform data to directly obtain the phase and amplitude of the annual harmonic; this decomposition can be performed pointwise. The second method is empirical orthogonal function (EOF) analysis, which extracts patterns of coherent variability in the data (Kutzbach 1967). The dominant spatial pattern (EOF1) explains 85% of the variability in tropical SST and 70% in tropical precipitation. By fitting a sinusoid to the principal component (PC) associated with the annual cycle, PC1, we obtain the amplitude and phase (Biasutti and Sobel 2009; Dwyer et al. 2012). Any change to PC1 of precipitation can be interpreted as a change in the timing or strength of the ITCZ movement or monsoonal precipitation (Fig. 1a), assuming that EOF1 changes little, an assumption we address below.

To create the SST forcing for the uniform warming (UW) experiment, we simply adjust the climatological SST by a fixed amount (3 K) for every month and at every

spatial grid point. For the seasonality experiment, we modify the phase and amplitude of the annual harmonic by first calculating the phase and amplitude of the annual harmonic of the control SST at each grid point using a Fourier transform and then either shifting the phase or amplifying the amplitude of the first harmonic before performing an inverse Fourier transform.

Alternatively, we could change the seasonality of all harmonics, instead of only the first. We test this effect by comparing two forced simulations differing only in the number of harmonics that are shifted. The difference between the two simulations is small for SST, precipitation, and other climate variables. We also tested the effect of changing the seasonality of sea ice in addition to SST. This led to large near-surface air temperature differences at high latitudes, but only small changes in precipitation at low latitudes.

To interpret the changes to PC1 as a shift or amplification of the timing of tropical precipitation, we require that the leading EOF pattern of each experiment be

TABLE 2. Multimodel mean changes in the annual mean, phase, and amplitude over ocean and land in the tropics (25°S–25°N) for the CMIP5 models (2080–99) minus (1980–99). Seasonal changes were calculated using an EOF analysis confined to either ocean or land. Confidence intervals indicate one standard error of the multimodel mean change and numbers in parentheses indicate the number of models projecting changes of the same sign as the mean for each quantity out of a total of 35 models.

	SST		Ocean precipitation		Land precipitation	
$\Delta$ annual mean	$2.9 \pm 0.1$ K	(35)	$0.2 \pm 0.0$ mm day <sup>-1</sup>	(35)	$0.1 \pm 0.0$ mm day <sup>-1</sup>	(27)
$\Delta$ amplitude	$4.2\% \pm 0.5\%$	(33)	$15.5\% \pm 1.1\%$	(34)	$8.2\% \pm 0.9\%$	(35)
$\Delta$ phase	$1.1 \pm 0.2$ days	(29)	$2.7 \pm 0.6$ days	(27)	$3.5 \pm 0.4$ days	(34)

similar to that of the control. In the simulations we perform, the EOF patterns are very similar. Figures 1b and 1c show the EOF1 pattern of precipitation for a phase delay of 15 days and an amplitude increase of 25%, respectively. The effect of the phase of SST on the EOF1 pattern of precipitation is small everywhere. Changing the amplitude of SST has a slightly larger effect on the EOF1 pattern of precipitation—it becomes stronger in some regions and weaker in others. Because the EOF1 patterns are normalized to the same global variance, an increased amplitude of precipitation will be expressed through the amplitude of PC1, not EOF1. We also verify our results by projecting the precipitation data for each forced run onto EOF1 of the control run and find only small differences from the standard method of projecting the precipitation data onto its own EOF1, leaving our conclusions unchanged.

### 3. CMIP5 results

In response to increased greenhouse gases in the RCP8.5 scenario, most CMIP5 models project not only annual mean increases to tropical temperature and precipitation, but also consistent changes to the seasonality of these quantities. We summarize the tropical CMIP5 changes for ocean and land in Table 2. All models predict increases in the annual mean of SST and oceanic precipitation with multimodel mean changes of 2.9 K and 0.2 mm day<sup>-1</sup>, respectively. There is less agreement among models on the sign of the annual mean change in terrestrial precipitation, which has a multimodel mean increase of 0.1 mm day<sup>-1</sup>. However, the amplitude increase and phase delay of precipitation are more robust over land than ocean—nearly all models agree on the sign of the changes to the seasonality of land precipitation. (We calculate changes in the annual cycle over land by limiting our EOF in spatial extent. This produces an EOF structure nearly identical to that of Fig. 1a, but with all of the power concentrated in land regions. A similar procedure is applied for the ocean.) In the multimodel mean, phase delays are larger over land (3.5 days) than ocean (2.7 days), although the amplitude increases are larger over ocean (15.5%) than land (8.2%). Seasonal changes

of SST are weaker than those for precipitation, although most models show an amplitude increase and phase delay.

Figure 2 shows the multimodel mean pattern of changes in SST and precipitation. Annual mean surface temperature increases throughout the tropics, especially on land, with the greatest ocean warming occurring on or near the equator (Fig. 2a). Increases in precipitation in the tropical oceans (Fig. 2b) mainly occur in regions with large climatological precipitation (Held and Soden 2006; Chou and Neelin 2004), as well as regions that have large increases in SST (Xie et al. 2010; Huang et al. 2013).

The amplitude of surface temperature (Fig. 2c) broadly increases throughout much of the tropics, aside from the western Pacific. This is in agreement with the tropical-wide amplitude increase of PC1 (Table 2), calculated by performing an EOF analysis over tropical SST (25°S–25°N). Changes in the amplitude of the annual cycle of precipitation, plotted in Fig. 2d, are positive along much of the equator, especially in the western Pacific and Indian Ocean, where the increase in amplitude is above 50%. These changes share some commonalities with the pattern of amplitude changes of SST in Fig. 2c (spatial correlation of 0.36) and to the annual mean SST change in Fig. 2a to a lesser extent (spatial correlation of 0.22). Many land monsoon regions also show increases in the amplitude of the annual cycle of precipitation, indicating an increase of summer precipitation relative to winter precipitation (Biasutti and Sobel 2009; Seth et al. 2011; Sobel and Camargo 2011; Seth et al. 2013). The intensification of the annual cycle of precipitation is mostly due to an increase during summer, with a smaller contribution from a reduction during winter (not shown).

The phase of surface temperature (Fig. 2e) delays for much of the NH tropical ocean off the equator, as well as in the eastern Pacific and Indian Ocean in the SH. While there are some regions of phase advance, the PC1 of tropical SST has a weak phase delay. Precipitation (Fig. 2f) is noisier, with strong regions of phase delay in the Caribbean Sea, Indian Ocean, and central Pacific and regions of phase advance in the tropical Atlantic and eastern Pacific. Projected changes of the timing of

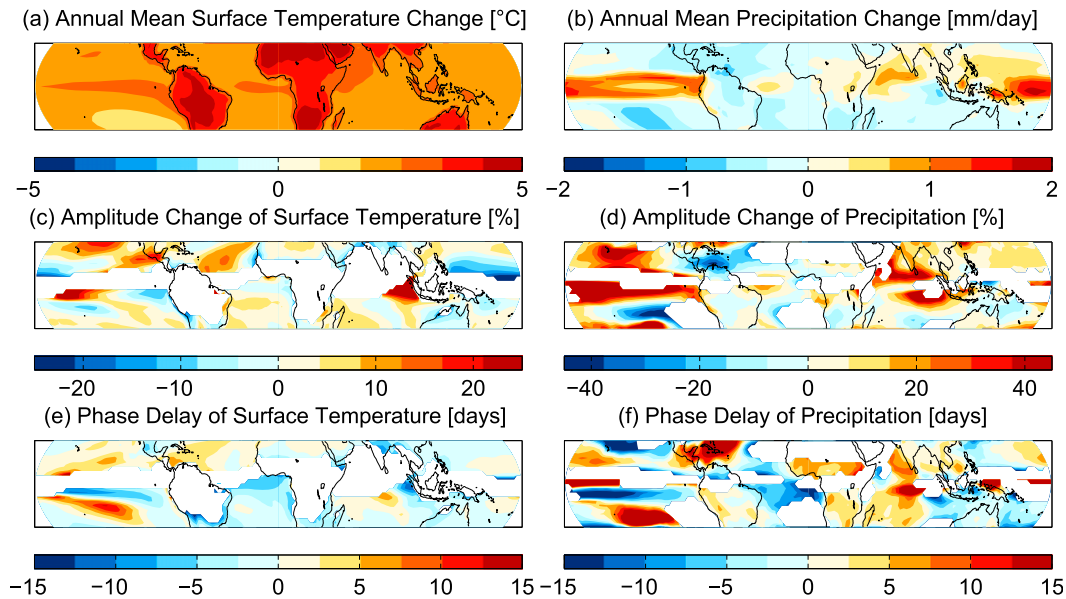


FIG. 2. The CMIP5 RCP8.5 multimodel mean change (2080–99) minus (1980–99) for: annual mean (a) temperature and (b) precipitation; amplitude change of the annual cycle of (c) temperature and (d) precipitation; and phase delay of the annual cycle of (e) temperature and (f) precipitation. Any location where the first harmonic makes up less than 80% or 50% of the total variance for temperature and precipitation, respectively, is not shaded. Additionally, for (d) and (f) only grid points that have at least an annual mean precipitation of 1 mm day<sup>-1</sup> are shaded.

precipitation in these regions have a larger magnitude than the tropical mean and may have important local consequences. Overall the PC1 of tropical oceanic precipitation shows a phase delay (Table 2).

We demonstrate the scatter between models in Fig. 3, which shows the seasonality changes of the zonal

mean SST and precipitation for the individual models and the multimodel mean. Amplitude changes of SST (Fig. 3a) are more tightly grouped than those of precipitation (Fig. 3b), although the changes in precipitation are larger. The same is true for the phase delays (Figs. 3c,d).

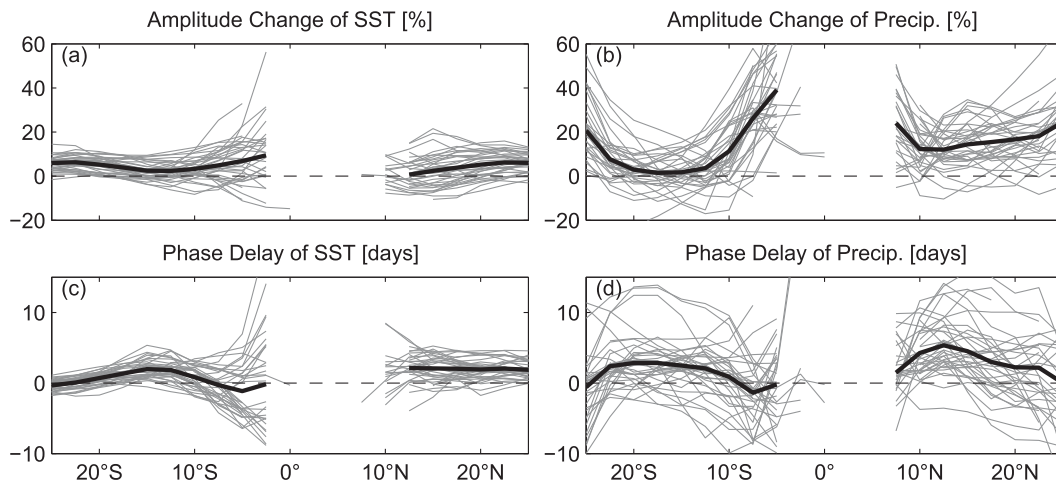


FIG. 3. Zonal mean changes for the CMIP5 models (2080–99) minus (1980–99) for: (a) the amplitude of SST, (b) the amplitude of precipitation, (c) the phase of SST, and (d) the phase of precipitation. The thick black line indicates the multimodel mean and the thin gray lines indicate the individual models. Values were calculated by first zonally averaging (over ocean for SST and over ocean and land for precipitation) and then calculating seasonal characteristics. Seasonal changes are only plotted where the annual harmonic is responsible for at least 85% of the total variance.

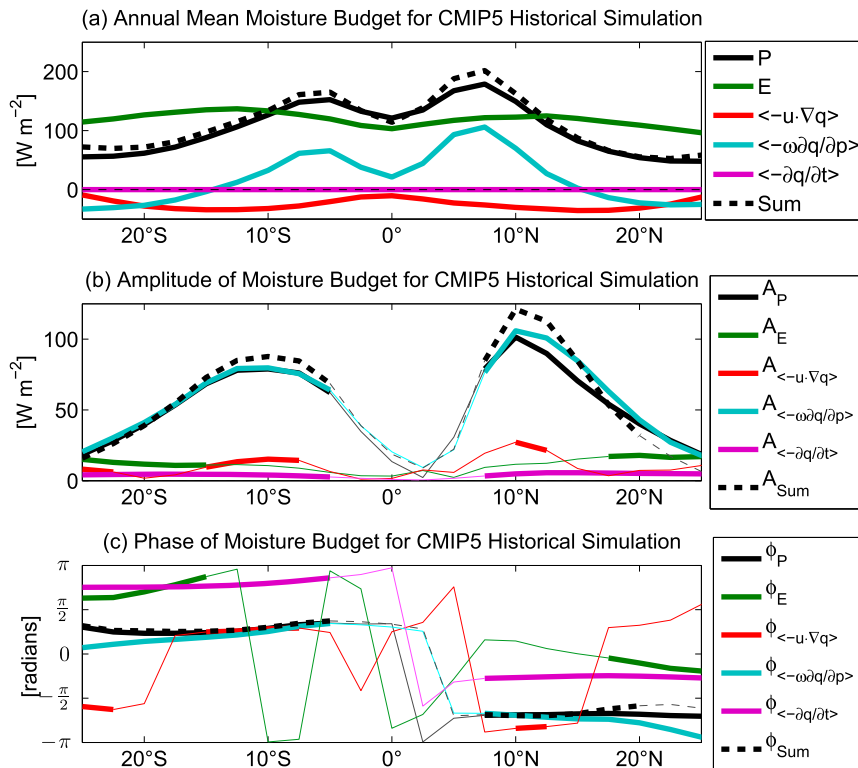


FIG. 4. (a) Annual mean, (b) amplitude, and (c) phase of the terms in the moisture budget [Eq. (3)] for the multimodel mean of the CMIP5 simulations. The solid thick black line is precipitation and the dashed thick black line is the sum of the other terms in the moisture budget. In (c), phases of  $\pi/2$  and  $-\pi/2$  correspond to maxima in April and October, respectively. Thick lines indicate where the annual harmonic is responsible for at least 85% of the total variance.

To investigate the nature of the seasonal precipitation changes in response to greenhouse gases, we analyze the moisture budget, following and extending previous work (Chou et al. 2007; Tan et al. 2008; Chou and Lan 2012; Huang et al. 2013). The moisture equation in flux form is

$$\langle \mathbf{V} \cdot (\mathbf{u}q) \rangle = E - P - \left\langle \frac{\partial q}{\partial t} \right\rangle, \quad (1)$$

where  $\mathbf{u}$  is the horizontal velocity,  $q$  is the specific humidity multiplied by the latent heat of vaporization,  $E$  is the evaporation, and  $P$  is the precipitation given in units of  $W m^{-2}$  ( $1 \text{ mm day}^{-1} \approx 28 W m^{-2}$ ). Angle brackets indicate a mass-weighted vertical integration from the surface to the tropopause:

$$\langle A \rangle = \frac{1}{g} \int_{p_{\text{sfc}}}^{p_{\text{trop}}} A dp, \quad (2)$$

where we use  $p_{\text{sfc}} = 1000 \text{ hPa}$  and  $p_{\text{trop}} = 250 \text{ hPa}$  for simplicity. Assuming that  $\omega = 0$  at the surface and the tropopause, then  $\langle \mathbf{V} \cdot (\mathbf{u}q) \rangle = \langle \omega \partial q / \partial p \rangle + \langle \mathbf{u} \cdot \nabla q \rangle$ , and the moisture budget can be written as

$$P = E + \langle -\mathbf{u} \cdot \nabla q \rangle + \left\langle -\omega \frac{\partial q}{\partial p} \right\rangle - \left\langle \frac{\partial q}{\partial t} \right\rangle. \quad (3)$$

We apply this decomposition to monthly data for the historical simulation for 1980–99 and plot the annual mean, amplitude, and phase of each component in Fig. 4. In the annual mean, the dominant balance averaged over the tropics is between  $P$  and  $E$  with a smaller contribution from  $\langle -\omega \partial q / \partial p \rangle$ , which becomes substantial in the deep tropics between 10°S and 10°N (Fig. 4a). The sum of the budget terms overestimates  $P$  by about 15% when averaged over the tropics, but shows better agreement in the deep tropics. Submonthly transients and surface effects likely account for most of this difference (Seager and Henderson 2013).

We also calculate the annual cycle of the budget. By zonally averaging each term in Eq. (3) and then calculating the temporal Fourier transform, we obtain the amplitude and phase of the first harmonic of each term in Eq. (3). We also calculate the phase and amplitude for the sum of the terms on the right-hand side of the equation since this is not simply the sum of the phases

or the sum of the amplitudes of each term (see [appendix A](#)). Analyzing the annual cycle of the budget allows us to visualize the annual cycle with two variables (amplitude and phase) rather than 12 monthly values, and to concisely determine which term best explains precipitation on seasonal time scales.

We plot the amplitudes of the terms in the moisture budget in [Fig. 4b](#). Thick lines are used for each term where the annual harmonic is responsible for at least 85% of the total variance, mostly outside of the deep tropics. The amplitude of precipitation is similar in latitudinal structure to the amplitude of the sum of the terms on the right-hand side of the budget but smaller. Because the amplitude of the sum of the terms is very similar to the amplitude of  $\langle -\omega\partial q/\partial p \rangle$ , we conclude that the primary balance of  $A_P$  is with  $A_{\langle -\omega\partial q/\partial p \rangle}$ , the amplitude of vertical moisture advection. These two terms are also in phase throughout the tropics as demonstrated in [Fig. 4c](#), indicating that the annual cycles of  $P$  and  $\langle -\omega\partial q/\partial p \rangle$  are in balance. The phases of the budget terms ([Fig. 4c](#)) also show that  $\phi_P$  is well described by the phase of the sum of the budget terms, except where the amplitude of the annual cycle is nearly zero. For the CMIP5 models this occurs around 2°N and poleward of around 20°N.

We investigate how  $A_P$ ,  $\phi_P$ , and other terms change in the RCP8.5 scenario by taking the Fourier transform of [Eq. \(3\)](#) and solving for  $A_P$  and  $\phi_P$ , while neglecting the moisture storage terms as these are of the same order as the residual of the budget. Assuming that the changes for each term between the RCP8.5 and control simulations (averaged over 2080–99 and 1980–99, respectively) are sufficiently small, we can write  $\Delta A_P$  and  $\Delta\phi_P$  as linear combinations of perturbations to the amplitudes and phases of each term in [Eq. \(3\)](#) (see [appendix A](#)). The contribution of each perturbation term to either  $\Delta A_P$  or  $\Delta\phi_P$  is the product of the perturbation term and a factor that depends on the relative amplitude and phases of the budget terms.

We plot the contribution from each term in [Fig. 5a](#). Here the thick lines represent where the changes in the amplitude of the annual cycle of precipitation were statistically different from zero at the 95% level (in this case everywhere), and the “×” markers at the bottom of the figure represent where the annual cycle of both precipitation and the sum of the moisture budget terms each capture at least 85% of the total variance. We focus on these regions in the analysis. The solid black line is the actual amplitude change in precipitation, and the dashed black line is the sum of the contributions from the perturbations to each term, which will resemble  $\Delta A_P$  if our decomposition is accurate. The value of  $\Delta A_P$  is positive throughout the tropics, and is largest near the

climatological maxima at 7.5°S and 7.5°N. The sum of perturbations matches  $\Delta A_P$  well except at 7.5°S and 15°N. The primary contribution to the sum comes from  $\Delta A_{\langle -\omega\partial q/\partial p \rangle}$ , the changes in the amplitude of the annual cycle of vertical moisture advection—unsurprising since this term dominates the budget in the control simulation ([Fig. 4b](#)). Similarly for phase,  $\Delta\phi_P$  is well described by the sum of the contributions from the individual terms in the tropics, although  $\Delta\phi_P$  is slightly larger than the sum in the NH ([Fig. 5b](#)). As before, the thick lines represent where changes in the phase are statistically significant. In the deep tropics, the annual cycle is weak so changes in the phase are neither well defined nor statistically significant. The largest contribution to balancing  $\Delta\phi_P$  comes from  $\Delta\phi_{\langle -\omega\partial q/\partial p \rangle}$ , although  $\Delta A_E$  also plays a role, especially in the SH and around 20°N.

Because of the strong balance in the annual cycle budget between  $P$  and  $\langle -\omega\partial q/\partial p \rangle$ , it is unsurprising that the changes in the amplitude of precipitation are best explained by similar changes in  $\Delta A_{\langle -\omega\partial q/\partial p \rangle}$ . To gain insight into what aspect of  $\langle -\omega\partial q/\partial p \rangle$  is changing in the RCP8.5 simulation we can decompose changes in  $\Delta A_{\langle -\omega\partial q/\partial p \rangle}$  and  $\phi_{\langle -\omega\partial q/\partial p \rangle}$  into contributions from six different terms: changes in the annual mean, amplitude, and phase of  $\omega$  and  $\partial q/\partial p$  (see [appendix B](#) for the full procedure).

First we consider the decomposition of  $\Delta A_{\langle -\omega\partial q/\partial p \rangle}$  and plot the results in [Fig. 5c](#). The sum of the decomposition is very similar to  $\Delta A_{\langle -\omega\partial q/\partial p \rangle}$ , even where the annual cycle is weak, validating our procedure and the neglect of small terms. For most of the tropics, the dominant contribution is from  $\partial\Delta\bar{q}/\partial p$ —an increase in the annual mean vertical gradient of water vapor. This effect is a thermodynamic consequence of the increase in temperature. Because the relative humidity stays roughly constant, the rise in mean temperature increases the moisture (i.e., specific humidity) throughout the troposphere, but especially in the lower atmosphere due to the Clausius–Clapeyron relation. The seasonally varying, ascending branch of the Hadley cell then converts the enhanced vertical moisture gradient into additional precipitation ([Held and Soden 2006](#)). Because vertical motion in the deep tropics is upward in the summer, the increase in  $\partial\bar{q}/\partial p$  results in an increase in  $A_P$ .

The other term that significantly affects  $\Delta A_{\langle -\omega\partial q/\partial p \rangle}$  is that due to the change in the amplitude of the circulation. This term contributes negatively to  $A_P$  for much of the tropics and partially compensates for the increase of  $\partial\Delta\bar{q}/\partial p$ . The negative contribution is associated with a reduction in the amplitude of the annual cycle of vertical motion due to some combination of reduced upward motion in summer and reduced subsidence in winter—indicative of a slowdown in the tropical meridional circulation throughout the annual cycle.

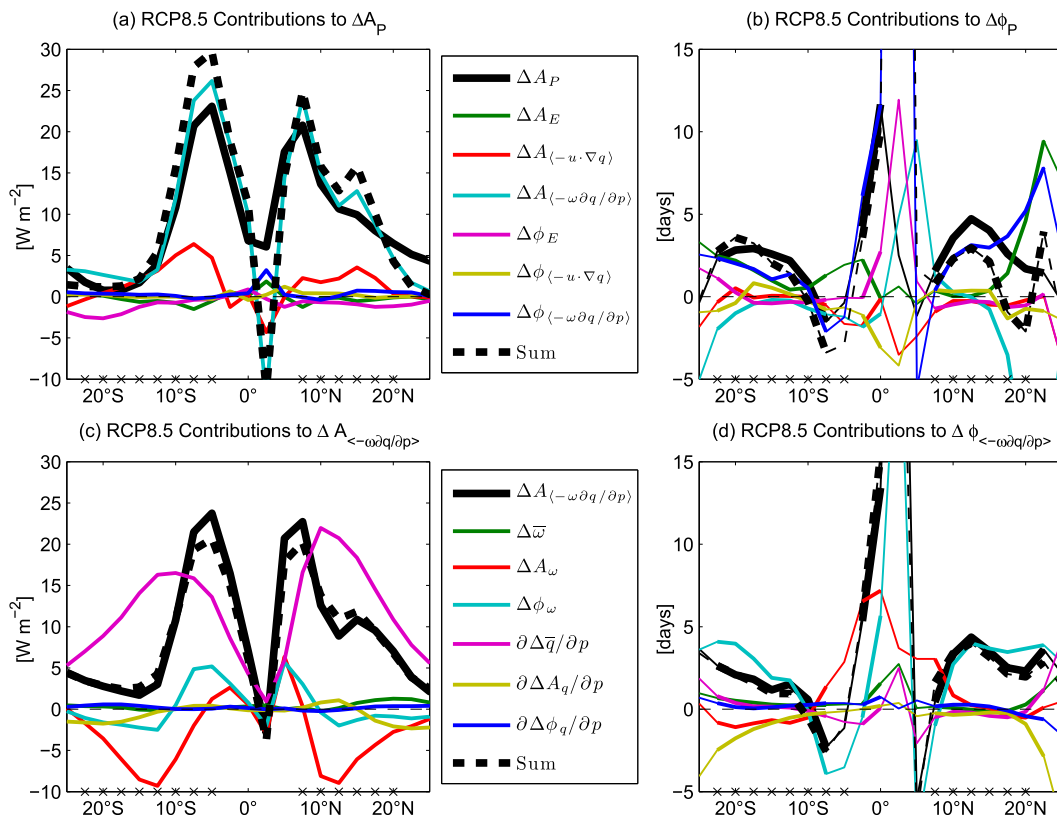


FIG. 5. (a) Contributions of terms to  $\Delta A_P$  in the RCP8.5 CMIP5 simulation as well as  $\Delta A_P$  itself (solid thick black line). The contribution of each term is the change in amplitude or phase multiplied by an appropriate factor (see appendix A). The sum of the contributions is given by the dashed thick black line. (b) As in (a), but for  $\Delta \phi_P$ . Further decomposition of (c)  $\Delta A_{\langle -\omega \partial q / \partial p \rangle}$  and (d)  $\Delta \phi_{\langle -\omega \partial q / \partial p \rangle}$  into changes related to the annual mean, amplitude, and phase of  $\omega$  and  $\partial q / \partial p$ . Data are plotted with a thinner line for latitudes at which the changes in the amplitude [in (a),(c)] or phase [in (b),(d)] are not statistically significant from zero at the 95% level. Latitudes for which the annual harmonics of both precipitation and the sum of the moisture budget terms makes up at least 85% of the total variance are marked with an  $\times$  on the x axis.

Previous studies have found similar results for changes due to increased greenhouse gases in the coupled models (Chou et al. 2007; Tan et al. 2008; Chou and Lan 2012; Huang et al. 2013). In particular, Tan et al. (2008) compared the changes in various terms of the moisture budget in summer and winter months. While they did not decompose changes in  $\langle -\omega \partial q / \partial p \rangle$  into annual mean and seasonal deviations, they found that changes in  $\langle -\omega \partial \Delta q / \partial p \rangle$  drove an increase in summer precipitation in the coupled models with some compensation from  $\langle -\Delta \omega \partial q / \partial p \rangle$ . We confirm these results in the CMIP5 models and extend previous studies by analyzing the phase response.

We decompose  $\Delta \phi_{\langle -\omega \partial q / \partial p \rangle}$  into a linear combination of terms, as we did with amplitude, and plot the results in Fig. 5d. While  $\Delta \phi_{\langle -\omega \partial q / \partial p \rangle}$  is not solely responsible for the changes in  $\Delta \phi_P$ , it is the largest contributor to  $\Delta \phi_P$ . Over the tropics,  $\Delta \phi_{\langle -\omega \partial q / \partial p \rangle}$  is mostly positive and mainly balanced by a phase delay of  $\omega$ . This result rules out

a thermodynamic explanation in terms of the Clausius–Clapeyron relation for the phase delay of precipitation, and indicates the importance of changes in the timing of circulation. The causes of the circulation changes are not yet known.

#### 4. Uniform warming experiment

To better understand the coupled response we turn to uncoupled simulations in which we can manipulate the SST. We begin by comparing the control CAM4 AGCM simulation to that of the historical CMIP5 simulations. In the annual mean, the various terms of the moisture budget of the control simulation (Fig. 6a) are similar to their counterparts in the CMIP5 models, except for stronger precipitation and vertical moisture advection in the deep tropics. There is also a larger interhemispheric asymmetry of precipitation and vertical moisture advection in the AGCM compared to the CMIP5 models,

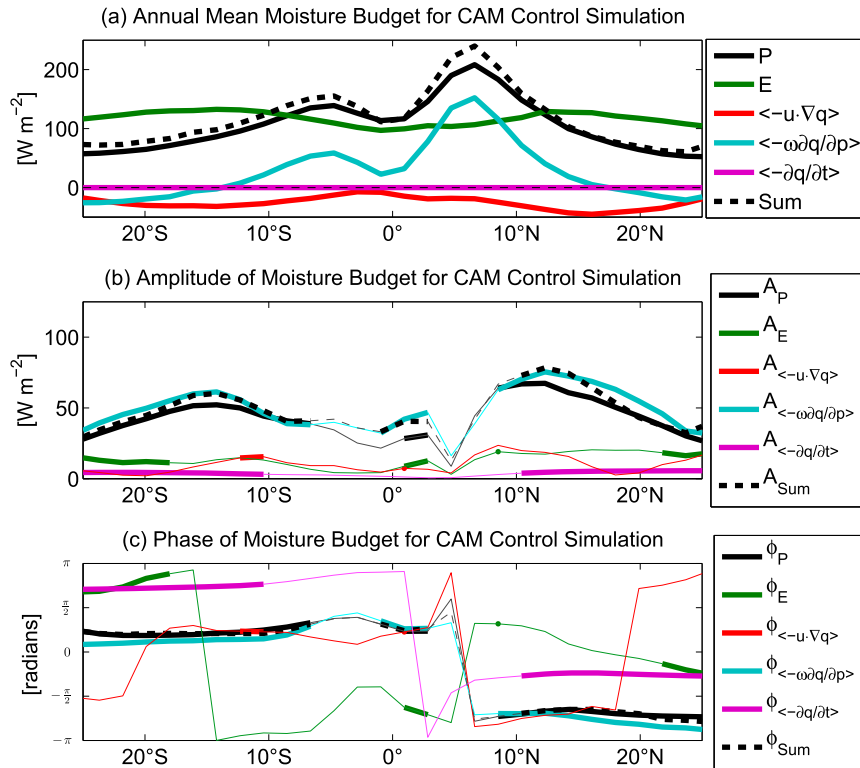


FIG. 6. As in Fig. 4, but for the AGCM control simulation for the (a) annual mean, (b) amplitude, and (c) phase of precipitation.

perhaps because of an erroneous double ITCZ in the coupled models (Lin 2007). The amplitude of the annual cycle in the control simulation (Fig. 6b) is weaker than that in the CMIP5 multimodel mean. Although there are two maxima in the amplitude of precipitation, they are weaker and less well defined than for the CMIP5 models. For both the annual mean and amplitude as well as for the phase (Fig. 6c, the sum of the decomposition of budget terms describes the precipitation well, including near the equator and poleward of 20°N, where it failed for the CMIP5 models. A comparison of the control simulations of CAM4 and CCSM4 (the coupled version of the AGCM model and included in the CMIP5 runs) shows nearly the same differences as those between CAM4 and the CMIP5 multimodel mean.

When the uncoupled model is forced with the climatological SST from the historical and RCP8.5 CCSM4 coupled simulations it captures the sign and approximate magnitude and latitudinal structure of the changes in the seasonality of precipitation and other budget terms as produced by the coupled model (not shown). Differences between the two simulations are likely due to some combination of differences in the atmospheric composition and in the background climate state, the damping effect of coupling on surface fluxes (Chiang

and Sobel 2002; Wu and Kirtman 2005, 2007; Emanuel and Sobel 2013), sampling error, and the fact that the CCSM4 is a transient simulation. While these differences prevent precise quantitative agreement between the coupled and uncoupled GCMs, the overall similarity of the results indicates that the uncoupled model is a useful tool for understanding the changes in the annual cycle in the coupled model.

Next we investigate the effects that a spatially uniform mean temperature increase has on the seasonal characteristics of precipitation in the UW experiment. We increase the SST by 3 K (Cess et al. 1990), a value almost identical to the increase of 2.9 K in the annual mean, tropical mean SST in the CMIP5 models between the end of the twenty-first and twentieth centuries. As a result of the SST warming, annual mean precipitation increases throughout the tropics and, according to the EOF method, the annual cycle of precipitation is amplified by 18.1% and its phase is delayed relative to the control simulation by 5.1 days.

We plot the latitudinal structure of the changes in the amplitude of the annual cycle of precipitation and related budget terms in the UW experiment in Fig. 7a. The amplitude of precipitation increases throughout the tropics, with the strongest increase around 15°N. The sum

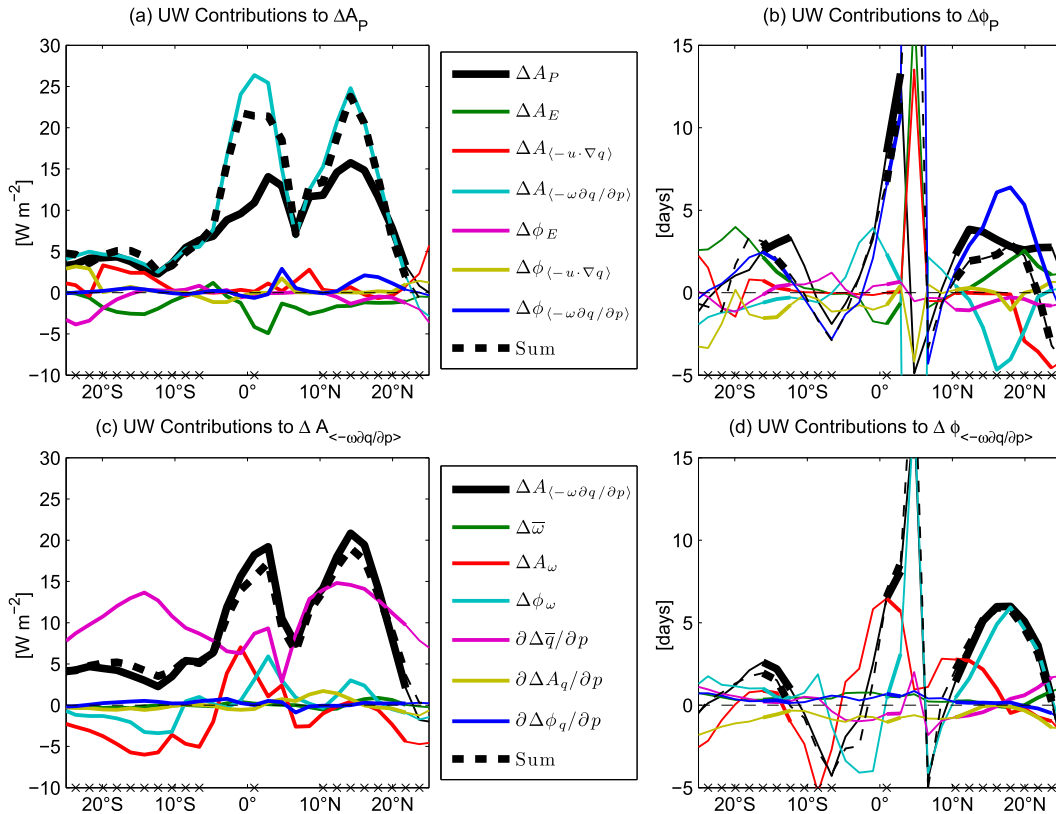


FIG. 7. As in Fig. 5, but for the UW simulation, showing contributions to (a)  $\Delta A_P$ , (b)  $\Delta \phi_P$ , (c)  $\Delta A_{\langle -\omega \partial q / \partial p \rangle}$ , and (d)  $\Delta \phi_{\langle -\omega \partial q / \partial p \rangle}$ .

of budget terms, dominated by  $\Delta A_{\langle -\omega \partial q / \partial p \rangle}$ , agrees with  $A_P$  where the annual cycle is strong, although it overestimates the maximum.

The phase changes of precipitation agree well with the sum of the contributions, except poleward of  $20^\circ$  (Fig. 7b), and show a delay at the equator and poleward of  $12^\circ$  in both hemispheres. This delay is statistically significant from zero in the NH, but not in much of the deep tropics or SH as indicated by the thin lines. When calculated via the EOF method over ocean or land in the entire tropics, precipitation has a clear, statistically significant phase delay, but is a noisier quantity at individual latitude bands. Still, the latitudinal structure is similar to that of the coupled models (cf. Fig. 5b). As with the CMIP5 models,  $\Delta \phi_{\langle -\omega \partial q / \partial p \rangle}$  plays a large role and  $\Delta A_E$  also contributes. Note that  $\Delta A_{\langle -\omega \partial q / \partial p \rangle}$  provides a negative contribution in both hemispheres, especially around  $15^\circ\text{N}$ .

Next we decompose the changes in  $\Delta A_{\langle -\omega \partial q / \partial p \rangle}$ , since this is the primary balance with  $\Delta A_P$  (Fig. 7c). As with the RCP8.5 CMIP5 models, the primary balance is with  $\partial \Delta \bar{q} / \partial p$ . The annual mean increase in moisture gradient contributes to the seasonal amplification of precipitation

in the same way as in the coupled models. Unlike in the RCP8.5 case, though, the latitudinal structure of these changes is not as symmetric about the equator. Similarly, a decrease in the amplitude of the circulation compensates for some of the increase in  $\partial \Delta \bar{q} / \partial p$ , but with a weaker and less symmetrical latitudinal structure about the equator than in the RCP8.5 case.

Returning to the budget for the phase changes, we decompose  $\Delta \phi_{\langle -\omega \partial q / \partial p \rangle}$  into a linear combination of terms (Fig. 7d). Here the decomposition works very well as the linear combination of decomposed terms is nearly identical to  $\Delta \phi_{\langle -\omega \partial q / \partial p \rangle}$ . The primary contribution comes from a delay in the phase of circulation, especially in the NH, with a smaller contribution coming from a change in the amplitude of circulation. These changes outweigh a negative contribution to the phase delay of precipitation from  $\Delta A_{\langle -\omega \partial q / \partial p \rangle}$ , which is mainly the result of the annual mean increase in moisture gradient.

Despite the differences between coupled models with realistic twenty-first-century forcings (including greenhouse gas changes and aerosols) and an AGCM with a uniform SST increase, there is much similarity in their seasonal precipitation responses. Both show an

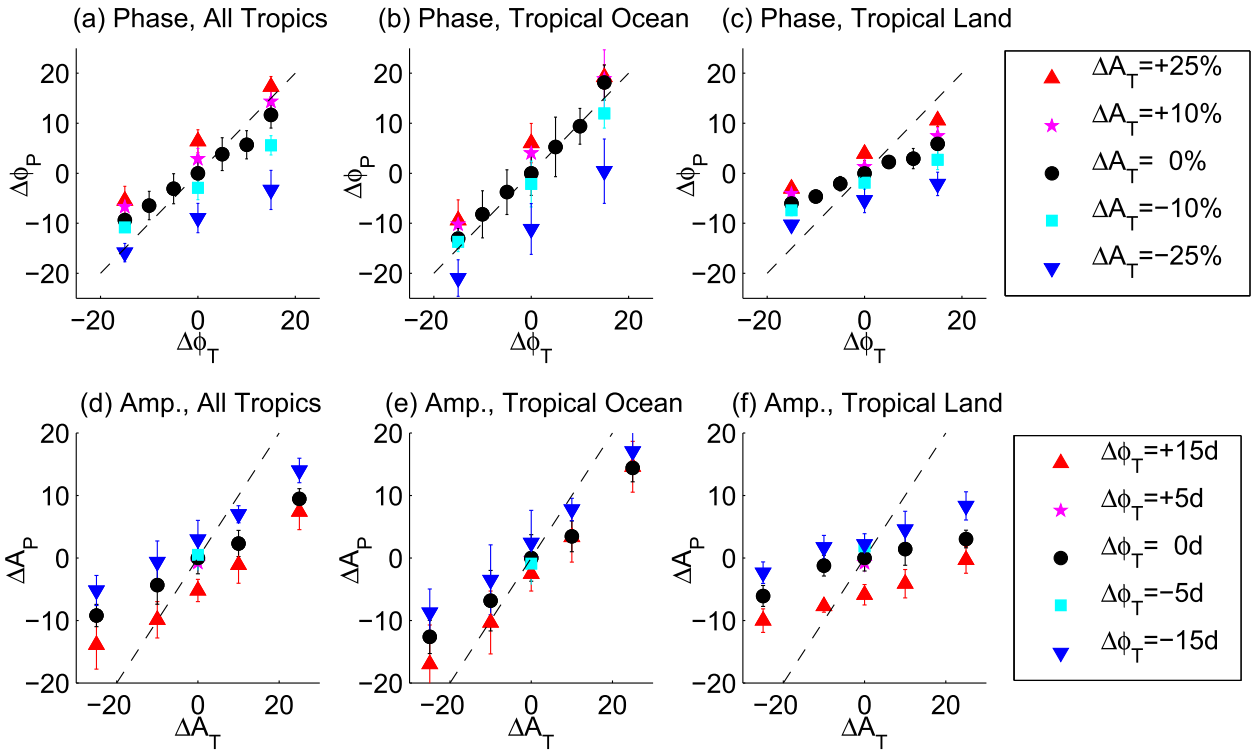


FIG. 8. Results of AGCM simulations with the seasonality of precipitation as a function of imposed seasonality of SST. The phase of precipitation vs the phase of SST for (a) the entire tropics, (b) tropical ocean, and (c) tropical land, with the colors representing the imposed amplitude of SST for each simulation. (d)–(f) As in (a)–(c), but for the amplitude of precipitation vs the amplitude of SST with colors representing the imposed phase of SST. Error bars represent one standard error.

amplification and phase delay in the annual cycle of precipitation in the tropics with similar latitudinal structure. Moreover, the terms that contribute to these seasonal changes are very similar between these simulations, indicating that the same processes may be at work. To summarize, an annual mean uniform warming in SST causes an amplification of the annual cycle of precipitation, mostly through the annual mean change in water vapor combined with the climatological seasonal circulation; it also causes a phase delay that is related to a phase delay in the circulation.

## 5. Modified seasonality experiment

In the second set of experiments, we investigate the effect that changing only the seasonal characteristics of SST has on the annual cycle of precipitation. We run seven simulations with amplitude as in the control run and phase shifts varying from a 15-day advance to a 15-day delay (see section 2 for details) and plot the resulting changes in the phase of precipitation as black circles in Fig. 8a. The results show that a delayed SST causes delayed precipitation and advanced SST causes

advanced precipitation. Moreover, the relationship between the phases of SST and precipitation is linear. This is the case even when the phase perturbations are imposed on simulations with a different amplitude of the annual cycle of SST (colored markers in Fig. 8a).

For all sets of simulations with identical changes in the amplitude of SST, the change in the phase of precipitation is weaker than the imposed change in the phase of SST (the slope of the linear relationship is less than one). This low sensitivity appears to be due to the presence of land. The phase of precipitation in Fig. 8a is calculated from a PC associated with an EOF structure that includes both land and ocean (Fig. 1). If we perform an EOF analysis with a domain limited to the ocean and calculate the seasonality of precipitation from its PC, the slope is nearly one, as in Fig. 8b. Likewise, when we limit our EOF analysis to precipitation over land (Fig. 8c) we find a slope that is close to zero. This is consistent with Biasutti et al. (2003, 2004), who found that the seasonality of precipitation primarily follows SST over ocean, but insolation over land.

As was the case for phase, the change in amplitude of the annual cycle of precipitation is linearly related with

a positive slope to the change in amplitude of the annual cycle of SST. Figure 8d shows the relationship holds for any set of simulations with the same phase of SST and varying amplitudes of SST, although again the slope is less than one. In this case, limiting the EOF to ocean (Fig. 8e) results in a slightly stronger sensitivity, but with a slope still less than one. We would expect a sensitivity of one if the relationship between SST and tropical oceanic precipitation were linear. In reality and in GCMs, the relationship between SST and precipitation is more complicated, as precipitation is suppressed in a convectively stable environment.

When we constrain the EOF to land (Fig. 8f), the slope is still greater than zero, but very small. Part of the reason for the shallow slope is because precipitation is positive definite. Near-zero winter precipitation is the case in many land-monsoon regions, such as the Sahel, South Asia, Australia, and South Africa. In these regions, anything more than a 10% increase in the amplitude of the annual cycle of precipitation would require an increase in the annual mean or changes in higher harmonics to prevent winter precipitation from becoming negative in the AGCM.

In addition to the direct forcing of phase on phase and amplitude on amplitude, there are cross-effects: the phase of SST affects the amplitude of precipitation and the amplitude of SST changes the phase of precipitation, as illustrated by the spread of the colored markers in Fig. 8. If we limit the EOF analysis to oceanic precipitation only (Figs. 8b,e), the effect remains with about the same magnitude as for the case with global precipitation (Figs. 8a,d). The effect is not an artifact of EOF analysis—it also exists when we perform our analysis with a Fourier transform of the data. If oceanic, tropical precipitation were entirely dependent on SST alone, we would not expect these cross-effects.

We interpret these effects as primarily due to the presence of land. Limiting the EOF to ocean does not eliminate the cross-effects because tropical convection can organize on large scales that cover both ocean and land for phenomena such as monsoons, inextricably linking the two domains. In this sense, oceanic precipitation is a function of both SST and insolation, the latter of which peaks earlier in the year.

The cross-effects can be understood mathematically by thinking of tropical precipitation  $P$  as a linear combination of insolation ( $I$ ) and SST ( $T$ ):  $P = \sigma I + \tau T$ , where  $\sigma$  and  $\tau$  give the relative strengths of  $I$  and  $T$  and ensure correct units. By writing this equation in seasonal form as  $A_P e^{-i\phi_P} = \sigma A_I + \tau A_T e^{-i\phi_T}$  (where  $A$  and  $\phi$  are the amplitude and phase lag from insolation of the annual cycle for the subscripted quantities) and solving for the seasonality of precipitation we find

$$A_P = \sqrt{\sigma^2 A_I^2 + \tau^2 A_T^2 + 2\sigma\tau A_I A_T \cos\phi_T}, \quad (4)$$

$$\phi_P = \arctan\left(\frac{\tau A_T \sin\phi_T}{\tau A_T \cos\phi_T + \sigma A_I}\right). \quad (5)$$

Assuming small changes to the phase and amplitude of SST, we can write the resulting changes to the phase and amplitude of precipitation as

$$\Delta A_P = \Delta A_T \left( \frac{\tau^2 A_T + \tau\sigma A_I \cos\phi_T}{A_P} \right) + \Delta\phi_T \left( \frac{-\tau\sigma A_I A_T \sin\phi_T}{A_P} \right), \quad (6)$$

$$\Delta\phi_P = \Delta A_T \left( \frac{\tau\sigma A_I \sin\phi_T}{A_P^2} \right) + \Delta\phi_T \left( \frac{\tau\sigma A_I A_T \cos\phi_T + \tau^2 A_T^2}{A_P^2} \right). \quad (7)$$

Since all of the amplitudes and phases are positive and  $\phi_T \approx 73$  days for tropically averaged SST, this model gives the expected result that delayed and amplified SST produces delayed and amplified precipitation. The model also predicts the presence of cross-effects with the right signs: a delayed SST leads to a weakened annual cycle of precipitation and an amplified SST leads to a delayed annual cycle of precipitation. The magnitude of these effects depends not only on the various unforced amplitudes and phases, but also on the relative importance of SST and insolation at forcing precipitation.

We also confirm that this is the case by running aquaplanet simulations, which have no land—only an ocean with an imposed seasonally varying SST—and no zonal asymmetries in the boundary conditions. As expected, in the aquaplanet simulations the direct effects are still present: delayed and amplified SST yields delayed and amplified precipitation, respectively. However, the cross-effects are smaller and no longer statistically significant at the 95% level. The effect that the amplitude of SST has on the phase of precipitation is reduced by 60% in the aquaplanet simulations and the effect that the phase of SST has on the amplitude of precipitation is reduced by 85%. Insolation still varies throughout the year, and has a phase-locked annual cycle of shortwave absorption in the atmosphere that may account for the remainder of the cross-effects. But when the effects of land and other zonal asymmetries are totally removed, the cross-effects diminish considerably.

We also repeat the budget analysis that we performed for the CMIP5 and UW simulations for a simulation

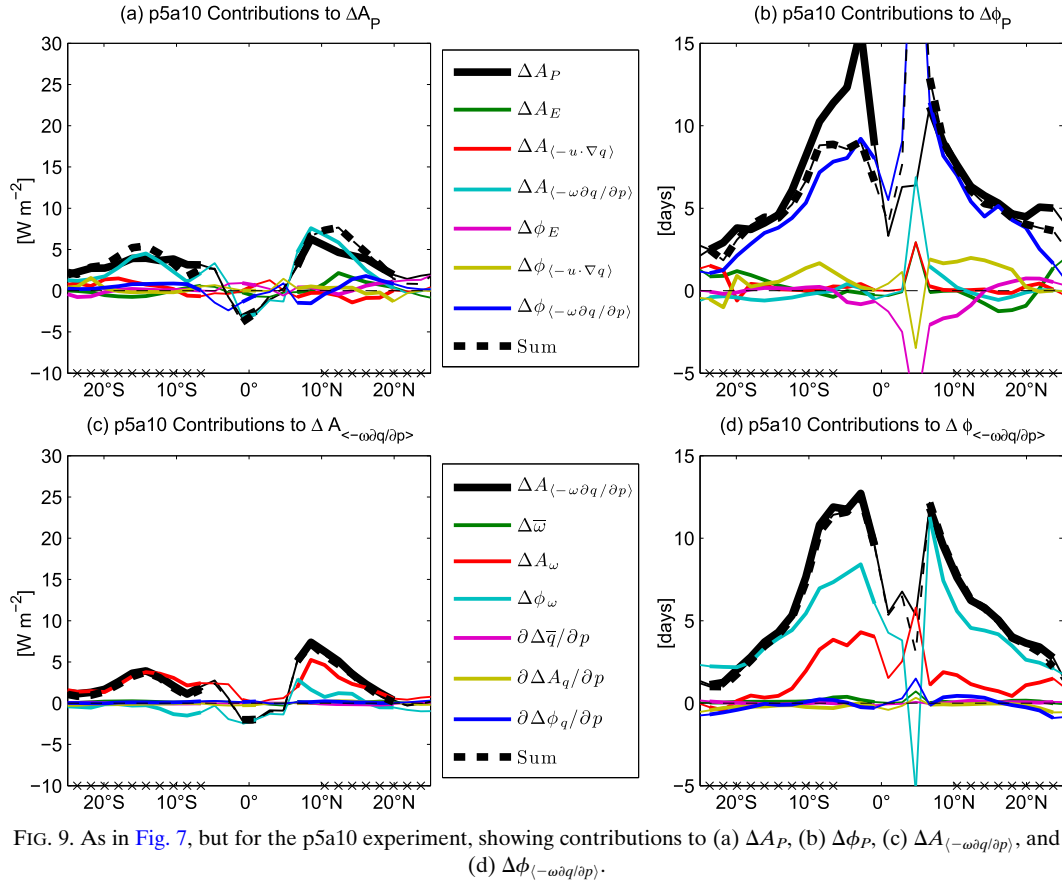


FIG. 9. As in Fig. 7, but for the p5a10 experiment, showing contributions to (a)  $\Delta A_P$ , (b)  $\Delta \phi_P$ , (c)  $\Delta A_{\langle -\omega \partial q / \partial p \rangle}$ , and (d)  $\Delta \phi_{\langle -\omega \partial q / \partial p \rangle}$ .

with a 5-day SST phase delay and a 10% SST amplitude increase (p5a10) and plot the results in Fig. 9. The chosen values of phase delay and amplitude increase to SST are exaggerated compared to the CMIP5 multimodel mean changes in order to obtain clearer results. In this simulation  $\Delta A_P$  increases throughout the tropics, but to a lesser degree than in the RCP8.5 and UW simulations. The increase is statistically significant, except in the deep tropics. The sum of the contributions generally agrees with the actual change in  $\Delta A_P$ , but overestimates the changes near the peaks. As in the other simulations, the primary contribution comes from  $\Delta A_{\langle -\omega \partial q / \partial p \rangle}$ . The change in the phase of precipitation is positive over the tropics, indicating a delay. Like the UW simulation, it is balanced by  $\Delta \phi_{\langle -\omega \partial q / \partial p \rangle}$  (Fig. 9b), but here with greater statistical significance.

When we decompose the changes to  $\Delta A_{\langle -\omega \partial q / \partial p \rangle}$  (Fig. 9c), we find that the sole contribution arises from a change in the amplitude of the circulation. In the RCP8.5 and UW simulations, by comparison, most of the change was due to the annual mean increase in moisture gradient, with a negative contribution from a change in the amplitude of circulation. Phase changes in

$\langle -\omega \partial q / \partial p \rangle$  (Fig. 9d) are also balanced by changes in the circulation—in this case mostly from a change in the phase of the circulation and somewhat from a change in the amplitude of  $\omega$ . In this simulation, the direct effect of the moisture change is unimportant for understanding the changes in the seasonality of precipitation. Instead the seasonal changes of SST are communicated to the precipitation via the circulation.

## 6. Comparison between AGCM experiments and CMIP5

To better understand the nature of the seasonal changes in precipitation in the CMIP5 models, we construct a simple, empirical model from the results of our AGCM simulations. For example, since the CMIP5 multimodel mean and the UW simulation both have almost identical mean temperature increases in the tropical average (2.9 K for CMIP5 and 3 K for the UW simulation), we can determine the amplitude and phase change in precipitation in the CMIP5 models due to an annual mean warming by using the results of the UW simulation. Because we know the change in the amplitude of

TABLE 3. Calculated changes in amplitude and phase in precipitation for both ocean and land given changes in the annual mean and annual cycle of SST in the CMIP5 models. We used the UW simulation to calculate the sensitivity of the amplitude and phase of precipitation to changes due to an annual mean SST increase and the sensitivity of the modified seasonality experiments to calculate the changes due to a phase or amplitude change of SST. Total calculated changes are the sum of the individual contributions. CMIP5 changes are taken from Table 2. Confidence intervals represent one standard error of the multimodel mean CMIP5 projections.

	Ocean		Land	
	Calculated $A_P$ (%)	Calculated $\phi_P$ (days)	Calculated $A_P$ (%)	Calculated $\phi_P$ (days)
$\overline{\Delta SST}_{\text{CMIP5}} = 2.9 \text{ K}$	$18.1 \pm 0.6$	$5.1 \pm 0.2$	$6.3 \pm 0.3$	$1.6 \pm 0.1$
$\Delta A_{\text{SST,CMIP5}} = 4.2\%$	$2.4 \pm 0.3$	$1.4 \pm 0.2$	$0.8 \pm 0.1$	$0.8 \pm 0.1$
$\Delta \phi_{\text{SST,CMIP5}} = 1.1 \text{ days}$	$-0.1 \pm 0.0$	$1.0 \pm 0.2$	$-0.3 \pm 0.0$	$0.4 \pm 0.1$
Total calculated	$20.4 \pm 0.8$	$7.4 \pm 0.3$	$6.8 \pm 0.3$	$2.8 \pm 0.1$
Actual CMIP5	$15.5 \pm 1.1$	$2.7 \pm 0.6$	$8.2 \pm 0.9$	$3.5 \pm 0.4$

temperature in the CMIP5 models and the sensitivity of changes in the amplitude of precipitation to changes in the amplitude of SST (the slope of the black dots in Fig. 8d), their product is the change of the amplitude of precipitation in the CMIP5 models due to  $\Delta A_T$ . Similarly, we can repeat this for phase as well as for the cross-effects (the effect of  $\Delta \phi_T$  on  $\Delta A_P$  and  $\Delta A_T$  on  $\Delta \phi_P$ ).

We express our model mathematically as

$$\begin{bmatrix} \Delta A_P \\ \Delta \phi_P \end{bmatrix} = \begin{bmatrix} C_{A_P, A_{\text{SST}}} & C_{A_P, \phi_{\text{SST}}} & C_{A_P, \overline{\Delta \text{SST}}} \\ C_{\phi_P, A_{\text{SST}}} & C_{\phi_P, \phi_{\text{SST}}} & C_{\phi_P, \overline{\Delta \text{SST}}} \end{bmatrix} \begin{bmatrix} \Delta A_{\text{SST}} \\ \Delta \phi_{\text{SST}} \\ \overline{\Delta \text{SST}} \end{bmatrix}, \quad (8)$$

where, for example,  $C_{A_P, A_{\text{SST}}}$  represents the change of the amplitude of precipitation due to the change in the amplitude of SST as derived from the AGCM simulations. The changes in the SST are taken from the CMIP5 models and when multiplied by the appropriate coefficients yield the calculated changes in the amplitude and phase of precipitation in the CMIP5 models.

There are some significant caveats to this method. We are using a model without an interactive ocean to interpret results from models with interactive oceans. This ignores any possibility that changes in the atmosphere may feed back on the seasonality of SST. It is possible that changes in the seasonality of SST are a consequence of changes in the seasonality of precipitation and not the other way around in the CMIP5 models. Additionally, there are differences between coupled and uncoupled versions of the same model even with the same SST. These differences suggest that, while useful, the AGCM is an imperfect tool to understand the GCM changes. Finally, we are not imposing the actual spatial pattern of annual mean or annual cycle changes of SST in our AGCM. Instead we impose a uniform change across the tropical oceans and calculate the results for the tropics as a whole.

We list the results in Table 3 for both ocean and land. Each entry in the table is the product of the change in SST multiplied by the appropriate coefficient in Eq. (8). For ocean, around 90% of the contribution to  $\Delta A_P$  comes from the annual mean increase of SST, with around 10% from the increase in  $\Delta A_T$  and a small negative contribution due to the cross-effect of  $\Delta \phi_T$ . As a whole, these contributions outweigh the actual measured increase in  $\Delta A_P$  by around 30%. Similarly, for  $\Delta \phi_P$  the largest contribution (5.1 days) is from the annual mean SST increase, while  $\Delta A_T$  contributes 1.4 days and  $\Delta \phi_T$  contributes only 1.0 days. Even though phase changes in precipitation are sensitive to phase changes in temperature, the phase delay of SST in CMIP5 is only 1.1 days, resulting in a relatively weak contribution to the phase delay of precipitation. Again the total changes constructed by this empirical model are larger than the actual CMIP5 changes, here by over a factor of 2–3.

Over land the results are similar, although each term is smaller than over ocean. As a result the sum of the inferred changes for  $\Delta A_P$  is 6.8%, very similar to the actual value for CMIP5 of 8.2%. For  $\Delta \phi_P$ , the sum of the contributions actually underestimates the total (2.8 days compared to 3.5 days). The better agreement over land compared to ocean suggests that coupling to a thermodynamically interactive lower boundary may be important. In our simulations, the land temperature is interactive, satisfying a consistent surface energy budget, while the ocean temperature is not. An interactive ocean mixed layer can respond locally to large-scale atmospheric influences in such a way as to mute or otherwise substantially alter the precipitation response compared to what would occur over an ocean surface with fixed SST (e.g., Chiang and Sobel 2002; Wu and Kirtman 2005, 2007; Emanuel and Sobel 2013).

Much of this study has focused on precipitation changes over ocean. Nevertheless, Table 2 indicates that the delays in the phase of precipitation are not only larger but also more robust over tropical land than over

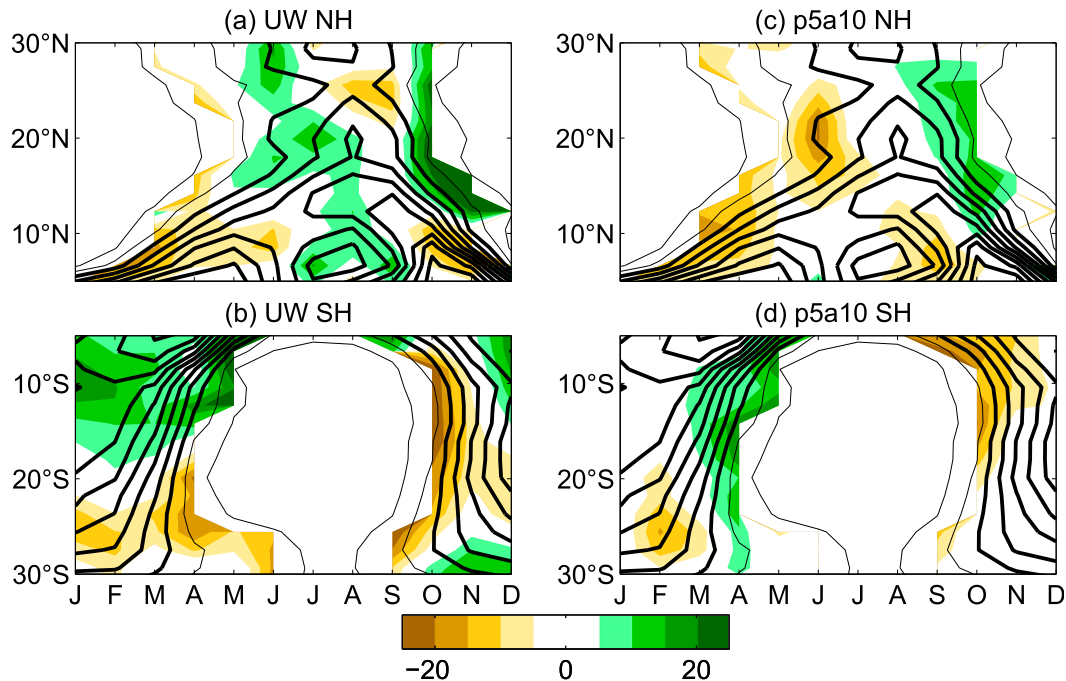


FIG. 10. Precipitation in land monsoon regions as a function of season and latitude in the control run (contours) and the percentage change (color shading) for the (a),(b) UW simulation and (c),(d) p5a10 simulation. In computing precipitation for (top) NH and (bottom) SH monsoons, the ocean has been masked out. Contour interval is  $1 \text{ mm day}^{-1}$  with thick contours representing precipitation  $\geq 3 \text{ mm day}^{-1}$ . The precipitation change is not shown for regions where the precipitation in the control run is  $< 1 \text{ mm day}^{-1}$ .

tropical ocean—34 of the 35 models project a phase delay over tropical land. Thus we now consider how the seasonality changes manifest over land in our idealized simulations and how they compare to changes in CMIP5 and those reported in the literature (Biasutti and Sobel 2009; Seth et al. 2011, 2013).

Our forced simulations produce changes in land monsoon regions that are similar to those of CMIP5. Specifically the UW simulation and the p5a10 simulation each show an amplification and phase delay in the annual cycle of precipitation in NH land monsoon regions, defined by averaging over land and over longitudes as in Seth et al. (2011).

Figures 10a and 10b show the CAM4 climatological precipitation (contour lines) and the percentage change in precipitation in the UW experiment (shading) for NH and SH monsoon regions, respectively. In both hemispheres the peak rainy season gets wetter, amplifying the annual cycle of precipitation. Additionally, an early season deficit and a late season excess of rain produce a phase delay. For the p5a10 simulation (Figs. 10c,d), the amplitude increase is milder than in the UW simulation, but the phase delay is of similar strength. The structure of the changes in both simulations bears much similarity, especially at the beginning and the end of the monsoon

season, despite the different nature of the imposed changes in SST between simulations.

## 7. Conclusions

We have studied the annual mean and seasonal response of tropical surface temperature and precipitation in the CMIP5 models to additional radiative forcing specified by the RCP8.5 scenario. We found, in addition to annual mean increases of SST and oceanic precipitation, and consistent with past studies, that the amplitudes of the annual cycles of SST and oceanic precipitation increased by 4.2% and 15.5% and that the phases were delayed by 1.1 days and 2.7 days, respectively.

From an analysis of the CMIP5 moisture budget we corroborate the work of previous studies (Tan et al. 2008; Huang et al. 2013) that found that the coupled model response of the amplitude of  $P$  is the result of an increase in the annual mean vertical moisture gradient due to the Clausius–Clapeyron relation. This additional water vapor is vertically advected in the summer months by the ascending branch of the Hadley cell. There is also a negative contribution to the amplitude of precipitation from a decrease in the amplitude of the annual cycle of vertical motion, consistent with a weakening of tropical

circulation. We also find the delay in the phase of precipitation is mostly balanced by a delay in the phase of the tropical circulation, although other terms like an increase in the amplitude of evaporation also contribute.

To better understand the precipitation response, we performed simulations with an AGCM forced by changes in the annual mean and annual cycle of SST. Increasing the annual mean SST everywhere by 3 K in the UW simulation caused not only an increase in annual mean tropical precipitation, but also amplification and a phase delay of the annual cycle of precipitation. We obtained seasonal precipitation changes of the same sign, albeit smaller, from the p5a10 simulation in which we left the mean value of SST unchanged, but amplified the annual cycle of SST by 10% and delayed it by 5 days. The changes in the CMIP5 models are better reproduced in the UW simulation than in the p5a10 simulation. A uniform SST warming produces amplitude changes in precipitation that are primarily balanced by an increase in the annual mean vertical gradient of moisture, just as in the coupled models. The p5a10 simulation, on the other hand, produces a weaker amplitude change (despite exaggerated forcing) that is due to an enhanced circulation rather than thermodynamic effects. Additionally, the magnitude and latitudinal structure of phase changes are more similar to the UW simulation than to the p5a10 simulation.

Because so many of the models have an amplification and delay in the annual cycle of precipitation, the mechanism responsible for this behavior is likely simple. The amplitude response can be explained by well-studied mechanisms: the increase in the annual mean vertical moisture gradient due to Clausius–Clapeyron and the slowdown in the circulation (Held and Soden 2006; Vecchi et al. 2006) (although here the slowdown is in the annual cycle and the Hadley cell, not the Walker cell). The phase response of precipitation is associated with a phase delay in the circulation. While we can rule out the possibility that the phase delay is a simple Clausius–Clapeyron response, we do not yet have a full explanation of the mechanism behind the delay.

The simulations in which we varied the phase and amplitude of SST demonstrated that seasonal changes to SST force seasonal changes in tropical precipitation of the same sign (i.e., delayed SST causes delayed precipitation and amplified SST causes amplified precipitation). These changes are communicated effectively by seasonal changes to the tropical circulation. These effects are not limited to ocean, either. Land monsoon regions are sensitive to the seasonal characteristics of SST in the same way as the ocean. Land is also responsible for cross-effects: changes to the phase of SST affect the amplitude of precipitation and changes to the amplitude of SST affect the phase of precipitation.

These AGCM simulations help inform our understanding of the nature of the seasonal changes in the GCMs. Though the lack of atmosphere–ocean coupling, a realistic spatial pattern of SST changes, and identical atmospheric forcing agents in the AGCM preclude exact quantitative agreement with the GCMs, the AGCM simulations indicate that an annual mean SST change is sufficient to induce most of the amplitude increase and phase delay in the annual cycle of precipitation in the GCMs. An important corollary of this result is that the seasonal changes in SST alone are not wholly responsible for the seasonal changes in precipitation in the CMIP5 ensemble.

*Acknowledgments.* This research was supported by NSF Grant AGS-0946849 and NASA Earth and Space Science Fellowship NNX11AL88H. We thank two anonymous reviewers for their helpful comments as well as Gus Correa for providing computer support for the simulations and Naomi Henderson and Haibo Liu for helping with the CMIP3 and CMIP5 datasets. We also wish to thank NCAR for allowing for public use of their GCM. We acknowledge the World Climate Research Programme’s Working Group on Coupled Modelling, which is responsible for CMIP, and we thank the climate modeling groups (listed in Table 1 of this paper) for producing and making available their model output. For CMIP the U.S. Department of Energy’s Program for Climate Model Diagnosis and Intercomparison provides coordinating support and led development of software infrastructure in partnership with the Global Organization for Earth System Science Portals.

## APPENDIX A

### Decomposition of Changes to the Moisture Budget

In this section we detail the procedure for expanding changes in the amplitude or phase of precipitation in terms of the amplitude or phase of evaporation, horizontal moisture advection, and vertical moisture advection. We begin by taking the Fourier transform of Eq. (3) budget and neglecting the moisture storage term:

$$A_P e^{-i\phi_P} = A_E e^{-i\phi_E} + A_{(-\mathbf{u}\cdot\nabla q)} e^{-i\phi_{(-\mathbf{u}\cdot\nabla q)}} + A_{(-\omega\partial q/\partial p)} e^{-i\phi_{(-\omega\partial q/\partial p)}}. \quad (\text{A1})$$

Solving this equation for the amplitude and phase of precipitation gives

$$A_P^2 = A_E^2 + A_{\langle -\mathbf{u}\cdot\nabla q \rangle}^2 + A_{\langle -\omega\partial q/\partial p \rangle}^2 + 2A_E A_{\langle -\mathbf{u}\cdot\nabla q \rangle} \cos(\phi_E - \phi_{\langle -\mathbf{u}\cdot\nabla q \rangle}) + 2A_E A_{\langle -\omega\partial q/\partial p \rangle} \cos(\phi_E - \phi_{\langle -\omega\partial q/\partial p \rangle}) + 2A_{\langle -\mathbf{u}\cdot\nabla q \rangle} A_{\langle -\omega\partial q/\partial p \rangle} \cos(\phi_{\langle -\mathbf{u}\cdot\nabla q \rangle} - \phi_{\langle -\omega\partial q/\partial p \rangle}), \tag{A2}$$

$$\tan\phi_P = \frac{A_E \sin\phi_E + A_{\langle -\mathbf{u}\cdot\nabla q \rangle} \sin\phi_{\langle -\mathbf{u}\cdot\nabla q \rangle} + A_{\langle -\omega\partial q/\partial p \rangle} \sin\phi_{\langle -\omega\partial q/\partial p \rangle}}{A_E \cos\phi_E + A_{\langle -\mathbf{u}\cdot\nabla q \rangle} \cos\phi_{\langle -\mathbf{u}\cdot\nabla q \rangle} + A_{\langle -\omega\partial q/\partial p \rangle} \cos\phi_{\langle -\omega\partial q/\partial p \rangle}}. \tag{A3}$$

Applying a small perturbation to Eqs. (A2) and (A3) and neglecting second-order terms results in a linear combination of perturbations to the phases and amplitudes of the budget terms.

$$\Delta A_P = \frac{1}{A_P} \times \begin{bmatrix} A_E + A_{\langle -\mathbf{u}\cdot\nabla q \rangle} \cos(\phi_E - \phi_{\langle -\mathbf{u}\cdot\nabla q \rangle}) + A_{\langle -\omega\partial q/\partial p \rangle} \cos(\phi_E - \phi_{\langle -\omega\partial q/\partial p \rangle}) \\ A_{\langle -\mathbf{u}\cdot\nabla q \rangle} + A_E \cos(\phi_{\langle -\mathbf{u}\cdot\nabla q \rangle} - \phi_E) + A_{\langle -\omega\partial q/\partial p \rangle} \cos(\phi_{\langle -\mathbf{u}\cdot\nabla q \rangle} - \phi_{\langle -\omega\partial q/\partial p \rangle}) \\ A_{\langle -\omega\partial q/\partial p \rangle} + A_E \cos(\phi_{\langle -\omega\partial q/\partial p \rangle} - \phi_E) + A_{\langle -\mathbf{u}\cdot\nabla q \rangle} \cos(\phi_{\langle -\omega\partial q/\partial p \rangle} - \phi_{\langle -\mathbf{u}\cdot\nabla q \rangle}) \\ -A_E A_{\langle -\mathbf{u}\cdot\nabla q \rangle} \sin(\phi_E - \phi_{\langle -\mathbf{u}\cdot\nabla q \rangle}) - A_E A_{\langle -\omega\partial q/\partial p \rangle} \sin(\phi_E - \phi_{\langle -\omega\partial q/\partial p \rangle}) \\ -A_{\langle -\mathbf{u}\cdot\nabla q \rangle} A_E \sin(\phi_{\langle -\mathbf{u}\cdot\nabla q \rangle} - \phi_E) - A_{\langle -\mathbf{u}\cdot\nabla q \rangle} A_{\langle -\omega\partial q/\partial p \rangle} \sin(\phi_{\langle -\mathbf{u}\cdot\nabla q \rangle} - \phi_{\langle -\omega\partial q/\partial p \rangle}) \\ -A_{\langle -\omega\partial q/\partial p \rangle} A_E \sin(\phi_{\langle -\omega\partial q/\partial p \rangle} - \phi_E) - A_{\langle -\omega\partial q/\partial p \rangle} A_{\langle -\mathbf{u}\cdot\nabla q \rangle} \sin(\phi_{\langle -\omega\partial q/\partial p \rangle} - \phi_{\langle -\mathbf{u}\cdot\nabla q \rangle}) \end{bmatrix}^T \begin{bmatrix} \Delta A_E \\ \Delta A_{\langle -\mathbf{u}\cdot\nabla q \rangle} \\ \Delta A_{\langle -\omega\partial q/\partial p \rangle} \\ \Delta\phi_E \\ \Delta\phi_{\langle -\mathbf{u}\cdot\nabla q \rangle} \\ \Delta\phi_{\langle -\omega\partial q/\partial p \rangle} \end{bmatrix} \tag{A4}$$

$$\Delta\phi_P = \frac{\cos^2\phi_P}{(A_E \cos\phi_E + A_{\langle -\mathbf{u}\cdot\nabla q \rangle} \cos\phi_{\langle -\mathbf{u}\cdot\nabla q \rangle} + A_{\langle -\omega\partial q/\partial p \rangle} \cos\phi_{\langle -\omega\partial q/\partial p \rangle})^2} \times \begin{bmatrix} A_{\langle -\mathbf{u}\cdot\nabla q \rangle} \sin(\phi_E - \phi_{\langle -\mathbf{u}\cdot\nabla q \rangle}) + A_{\langle -\omega\partial q/\partial p \rangle} \sin(\phi_E - \phi_{\langle -\omega\partial q/\partial p \rangle}) \\ A_E \sin(\phi_{\langle -\mathbf{u}\cdot\nabla q \rangle} - \phi_E) + A_{\langle -\omega\partial q/\partial p \rangle} \sin(\phi_{\langle -\mathbf{u}\cdot\nabla q \rangle} - \phi_{\langle -\omega\partial q/\partial p \rangle}) \\ A_E \sin(\phi_{\langle -\omega\partial q/\partial p \rangle} - \phi_E) + A_{\langle -\mathbf{u}\cdot\nabla q \rangle} \sin(\phi_{\langle -\omega\partial q/\partial p \rangle} - \phi_{\langle -\mathbf{u}\cdot\nabla q \rangle}) \\ A_E^2 + A_E A_{\langle -\mathbf{u}\cdot\nabla q \rangle} \cos(\phi_E - \phi_{\langle -\mathbf{u}\cdot\nabla q \rangle}) + A_E A_{\langle -\omega\partial q/\partial p \rangle} \cos(\phi_E - \phi_{\langle -\omega\partial q/\partial p \rangle}) \\ A_{\langle -\mathbf{u}\cdot\nabla q \rangle}^2 + A_{\langle -\mathbf{u}\cdot\nabla q \rangle} A_E \cos(\phi_{\langle -\mathbf{u}\cdot\nabla q \rangle} - \phi_E) + A_{\langle -\mathbf{u}\cdot\nabla q \rangle} A_{\langle -\omega\partial q/\partial p \rangle} \cos(\phi_{\langle -\mathbf{u}\cdot\nabla q \rangle} - \phi_{\langle -\omega\partial q/\partial p \rangle}) \\ A_{\langle -\omega\partial q/\partial p \rangle}^2 + A_{\langle -\omega\partial q/\partial p \rangle} A_E \cos(\phi_{\langle -\omega\partial q/\partial p \rangle} - \phi_E) + A_{\langle -\omega\partial q/\partial p \rangle} A_{\langle -\mathbf{u}\cdot\nabla q \rangle} \cos(\phi_{\langle -\omega\partial q/\partial p \rangle} - \phi_{\langle -\mathbf{u}\cdot\nabla q \rangle}) \end{bmatrix}^T \times \begin{bmatrix} \Delta A_E \\ \Delta A_{\langle -\mathbf{u}\cdot\nabla q \rangle} \\ \Delta A_{\langle -\omega\partial q/\partial p \rangle} \\ \Delta\phi_E \\ \Delta\phi_{\langle -\mathbf{u}\cdot\nabla q \rangle} \\ \Delta\phi_{\langle -\omega\partial q/\partial p \rangle} \end{bmatrix} \tag{A5}$$

## APPENDIX B

**Decomposition of the Vertical Moisture Advection Term**

Below we decompose  $A_{\langle-\omega\partial q/\partial p\rangle}$  and  $\phi_{\langle-\omega\partial q/\partial p\rangle}$  into changes in the annual mean, amplitude, and phase of  $\omega$  and  $\partial q/\partial p$ . We begin by separating the annual mean and deviations from the annual mean

$$\left\langle \omega \frac{\partial q}{\partial p} \right\rangle = \left\langle (\overline{\omega} + \omega') \left( \frac{\partial \overline{q}}{\partial p} + \frac{\partial q'}{\partial p} \right) \right\rangle, \quad (\text{B1})$$

where the overline indicates an annual mean and the prime indicates a deviation from the annual mean. We expand around small changes to this expression

$$\begin{aligned} \Delta = \left\langle \omega \frac{\partial q}{\partial p} \right\rangle &= \left\langle \Delta \overline{\omega} \frac{\partial \overline{q}}{\partial p} + \overline{\omega} \frac{\partial \Delta \overline{q}}{\partial p} + \Delta \overline{\omega} \frac{\partial q'}{\partial p} + \overline{\omega} \frac{\partial \Delta q'}{\partial p} \right. \\ &\quad \left. + \Delta \omega' \frac{\partial \overline{q}}{\partial p} + \omega' \frac{\partial \Delta \overline{q}}{\partial p} + \Delta \omega' \frac{\partial q'}{\partial p} + \omega' \frac{\partial \Delta q'}{\partial p} \right\rangle, \end{aligned} \quad (\text{B2})$$

where we have neglected second-order terms, an assumption that we will show below is valid. Next we take the Fourier transform of this equation, as indicated by curly braces:

$$\begin{aligned} \left\{ \Delta \left\langle \omega \frac{\partial q}{\partial p} \right\rangle \right\} &= \left\langle \Delta \overline{\omega} \frac{\partial \{q'\}}{\partial p} \right\rangle + \left\langle \overline{\omega} \frac{\partial \{\Delta q'\}}{\partial p} \right\rangle \\ &\quad + \left\langle \{\Delta \omega'\} \frac{\partial \overline{q}}{\partial p} \right\rangle + \left\langle \{\omega'\} \frac{\partial \Delta \overline{q}}{\partial p} \right\rangle. \end{aligned} \quad (\text{B3})$$

We have neglected the first two and last two terms of Eq. (B2), the former because the annual mean does not project onto the annual cycle, and the latter because the product of the two terms, each of which has its maximal variance at the annual harmonic, has its maximum variance at the semiannual harmonic. To determine the exact contribution of the phases and amplitudes of the terms in Eq. (B3) we perform a similar procedure as before to decompose the effects as a linear combination of perturbation terms. By taking the Fourier transform of Eq. (B3), we obtain

$$\begin{aligned} (\Delta A_{\langle-\omega\partial q/\partial p\rangle} - iA_{\langle-\omega\partial q/\partial p\rangle} \Delta \phi_{\langle-\omega\partial q/\partial p\rangle}) e^{-i\phi_{\langle-\omega\partial q/\partial p\rangle}} &= (\Delta A_{\langle-\Delta \overline{\omega}\partial\{q'\}/\partial p\rangle} - iA_{\langle-\Delta \overline{\omega}\partial\{q'\}/\partial p\rangle} \Delta \phi_{\langle-\Delta \overline{\omega}\partial\{q'\}/\partial p\rangle}) e^{-i\phi_{\langle-\Delta \overline{\omega}\partial\{q'\}/\partial p\rangle}} \\ &\quad + (\Delta A_{\langle-\overline{\omega}\partial\{\Delta q'\}/\partial p\rangle} - iA_{\langle-\overline{\omega}\partial\{\Delta q'\}/\partial p\rangle} \Delta \phi_{\langle-\overline{\omega}\partial\{\Delta q'\}/\partial p\rangle}) e^{-i\phi_{\langle-\overline{\omega}\partial\{\Delta q'\}/\partial p\rangle}} + (\Delta A_{\langle-\{\Delta \omega'\}\partial \overline{q}/\partial p\rangle} \\ &\quad - iA_{\langle-\{\Delta \omega'\}\partial \overline{q}/\partial p\rangle} \Delta \phi_{\langle-\{\Delta \omega'\}\partial \overline{q}/\partial p\rangle}) e^{-i\phi_{\langle-\{\Delta \omega'\}\partial \overline{q}/\partial p\rangle}} + (\Delta A_{\langle-\{\omega'\}\partial \Delta \overline{q}/\partial p\rangle} - iA_{\langle-\{\omega'\}\partial \Delta \overline{q}/\partial p\rangle} \Delta \phi_{\langle-\{\omega'\}\partial \Delta \overline{q}/\partial p\rangle}) e^{-i\phi_{\langle-\{\omega'\}\partial \Delta \overline{q}/\partial p\rangle}}, \end{aligned} \quad (\text{B4})$$

where, for example,  $\Delta A_{\langle-\overline{\omega}\partial\{q'\}/\partial p\rangle}$  represents the change in amplitude of  $\langle-\Delta \overline{\omega}\partial\{q'\}/\partial p\rangle$  due to a change in the annual mean of  $\omega$ . Because  $\Delta \overline{\omega}$  in  $\langle-\Delta \overline{\omega}\partial\{q'\}/\partial p\rangle$  is multiplied by the vertical moisture gradient at each level

and vertically integrated, changes in  $\overline{\omega}$  can alter the amplitude or phase of  $\langle-\Delta \overline{\omega}\partial\{q'\}/\partial p\rangle$ .

Solving Eq. (B4) for  $\Delta A_{\langle-\omega\partial q/\partial p\rangle}$  and  $\Delta \phi_{\langle-\omega\partial q/\partial p\rangle}$  separately yields the following:

$$\Delta A_{\langle-\omega\partial q/\partial p\rangle} = \begin{bmatrix} \cos(\phi_{\langle-\omega\partial q/\partial p\rangle} - \phi_{\langle-\Delta \overline{\omega}\partial\{q'\}/\partial p\rangle}) \\ \cos(\phi_{\langle-\omega\partial q/\partial p\rangle} - \phi_{\langle-\overline{\omega}\partial\{\Delta q'\}/\partial p\rangle}) \\ \cos(\phi_{\langle-\omega\partial q/\partial p\rangle} - \phi_{\langle-\{\Delta \omega'\}\partial \overline{q}/\partial p\rangle}) \\ \cos(\phi_{\langle-\omega\partial q/\partial p\rangle} - \phi_{\langle-\{\omega'\}\partial \Delta \overline{q}/\partial p\rangle}) \\ A_{\langle-\Delta \overline{\omega}\partial\{q'\}/\partial p\rangle} \sin(\phi_{\langle-\omega\partial q/\partial p\rangle} - \phi_{\langle-\Delta \overline{\omega}\partial\{q'\}/\partial p\rangle}) \\ A_{\langle-\overline{\omega}\partial\{\Delta q'\}/\partial p\rangle} \sin(\phi_{\langle-\omega\partial q/\partial p\rangle} - \phi_{\langle-\overline{\omega}\partial\{\Delta q'\}/\partial p\rangle}) \\ A_{\langle-\{\Delta \omega'\}\partial \overline{q}/\partial p\rangle} \sin(\phi_{\langle-\omega\partial q/\partial p\rangle} - \phi_{\langle-\{\Delta \omega'\}\partial \overline{q}/\partial p\rangle}) \\ A_{\langle-\{\omega'\}\partial \Delta \overline{q}/\partial p\rangle} \sin(\phi_{\langle-\omega\partial q/\partial p\rangle} - \phi_{\langle-\{\omega'\}\partial \Delta \overline{q}/\partial p\rangle}) \end{bmatrix}^T \begin{bmatrix} \Delta A_{\langle-\Delta \overline{\omega}\partial\{q'\}/\partial p\rangle} \\ \Delta A_{\langle-\overline{\omega}\partial\{\Delta q'\}/\partial p\rangle} \\ \Delta A_{\langle-\{\Delta \omega'\}\partial \overline{q}/\partial p\rangle} \\ \Delta A_{\langle-\{\omega'\}\partial \Delta \overline{q}/\partial p\rangle} \\ \Delta \phi_{\langle-\Delta \overline{\omega}\partial\{q'\}/\partial p\rangle} \\ \Delta \phi_{\langle-\overline{\omega}\partial\{\Delta q'\}/\partial p\rangle} \\ \Delta \phi_{\langle-\{\Delta \omega'\}\partial \overline{q}/\partial p\rangle} \\ \Delta \phi_{\langle-\{\omega'\}\partial \Delta \overline{q}/\partial p\rangle} \end{bmatrix} \quad (\text{B5})$$

$$\Delta\phi_{\langle-\omega\partial q/\partial p\rangle} = \frac{1}{A_{\langle-\omega\partial q/\partial p\rangle}} \begin{bmatrix} \sin(\phi_{\langle-\Delta\bar{\omega}\partial\{q'\}/\partial p\rangle} - \phi_{\langle-\omega\partial q/\partial p\rangle}) \\ \sin(\phi_{\langle-\bar{\omega}\partial\{\Delta q'\}/\partial p\rangle} - \phi_{\langle-\omega\partial q/\partial p\rangle}) \\ \sin(\phi_{\langle-\{\Delta\omega'\}\partial\bar{q}/\partial p\rangle} - \phi_{\langle-\omega\partial q/\partial p\rangle}) \\ \sin(\phi_{\langle-\{\omega'\}\partial\Delta\bar{q}/\partial p\rangle} - \phi_{\langle-\omega\partial q/\partial p\rangle}) \\ A_{\langle-\Delta\bar{\omega}\partial\{q'\}/\partial p\rangle} \cos(\phi_{\langle-\Delta\bar{\omega}\partial\{q'\}/\partial p\rangle} - \phi_{\langle-\omega\partial q/\partial p\rangle}) \\ A_{\langle-\bar{\omega}\partial\{\Delta q'\}/\partial p\rangle} \cos(\phi_{\langle-\bar{\omega}\partial\{\Delta q'\}/\partial p\rangle} - \phi_{\langle-\omega\partial q/\partial p\rangle}) \\ A_{\langle-\{\Delta\omega'\}\partial\bar{q}/\partial p\rangle} \cos(\phi_{\langle-\{\Delta\omega'\}\partial\bar{q}/\partial p\rangle} - \phi_{\langle-\omega\partial q/\partial p\rangle}) \\ A_{\langle-\{\omega'\}\partial\Delta\bar{q}/\partial p\rangle} \cos(\phi_{\langle-\{\omega'\}\partial\Delta\bar{q}/\partial p\rangle} - \phi_{\langle-\omega\partial q/\partial p\rangle}) \end{bmatrix}^T \begin{bmatrix} \Delta A_{\langle-\Delta\bar{\omega}\partial\{q'\}/\partial p\rangle} \\ \Delta A_{\langle-\bar{\omega}\partial\{\Delta q'\}/\partial p\rangle} \\ \Delta A_{\langle-\{\Delta\omega'\}\partial\bar{q}/\partial p\rangle} \\ \Delta A_{\langle-\{\omega'\}\partial\Delta\bar{q}/\partial p\rangle} \\ \Delta\phi_{\langle-\Delta\bar{\omega}\partial\{q'\}/\partial p\rangle} \\ \Delta\phi_{\langle-\bar{\omega}\partial\{\Delta q'\}/\partial p\rangle} \\ \Delta\phi_{\langle-\{\Delta\omega'\}\partial\bar{q}/\partial p\rangle} \\ \Delta\phi_{\langle-\{\omega'\}\partial\Delta\bar{q}/\partial p\rangle} \end{bmatrix} \quad (B6)$$

Since we are interested in what effect the various changes of annual mean, amplitude, and phase of  $\omega$  and  $\partial q/\partial p$  have on  $\langle-\omega\partial q/\partial p\rangle$ , we further decompose the terms  $A_{\langle-\bar{\omega}\partial\{\Delta q'\}/\partial p\rangle}$ ,  $A_{\langle-\{\Delta\omega'\}\partial\bar{q}/\partial p\rangle}$ ,  $\phi_{\langle-\bar{\omega}\partial\{\Delta q'\}/\partial p\rangle}$ , and  $\phi_{\langle-\{\Delta\omega'\}\partial\bar{q}/\partial p\rangle}$  each into separate terms relating to the change in amplitude or phase of  $\partial q/\partial p$  or  $\omega$  as follows:

$$\Delta A_{\langle-\bar{\omega}\partial\{\Delta q'\}/\partial p\rangle} = \Delta A_{\langle-\bar{\omega}\partial\{\Delta q'\}/\partial p\rangle;\Delta A_{\partial q/\partial p}} + \Delta A_{\langle-\bar{\omega}\partial\{\Delta q'\}/\partial p\rangle;\Delta\phi_{\partial q/\partial p}}, \quad (B7)$$

$$\Delta A_{\langle-\{\Delta\omega'\}\partial\bar{q}/\partial p\rangle} = \Delta A_{\langle-\{\Delta\omega'\}\partial\bar{q}/\partial p\rangle;\Delta A_{\omega}} + \Delta A_{\langle-\{\Delta\omega'\}\partial\bar{q}/\partial p\rangle;\Delta\phi_{\omega}}, \quad (B8)$$

$$\Delta\phi_{\langle-\bar{\omega}\partial\{\Delta q'\}/\partial p\rangle} = \Delta\phi_{\langle-\bar{\omega}\partial\{\Delta q'\}/\partial p\rangle;\Delta A_{\partial q/\partial p}} + \Delta\phi_{\langle-\bar{\omega}\partial\{\Delta q'\}/\partial p\rangle;\Delta\phi_{\partial q/\partial p}}, \quad (B9)$$

$$\Delta\phi_{\langle-\{\Delta\omega'\}\partial\bar{q}/\partial p\rangle} = \Delta\phi_{\langle-\{\Delta\omega'\}\partial\bar{q}/\partial p\rangle;\Delta A_{\omega}} + \Delta\phi_{\langle-\{\Delta\omega'\}\partial\bar{q}/\partial p\rangle;\Delta\phi_{\omega}}, \quad (B10)$$

where, for example,  $\Delta A_{\langle-\bar{\omega}\partial\{\Delta q'\}/\partial p\rangle;\Delta A_{\partial q/\partial p}}$  is the effect of a change in the amplitude of  $\partial q/\partial p$  on  $\Delta A_{\langle-\bar{\omega}\partial\{\Delta q'\}/\partial p\rangle}$ . With this in mind we can write the effect that changes in various components changes of  $\omega$  and  $q$  have on  $A_{\langle-\omega\partial q/\partial p\rangle}$  and  $\phi_{\langle-\omega\partial q/\partial p\rangle}$  as follows:

$$\begin{bmatrix} \Delta A_{\langle-\omega\partial q/\partial p\rangle;\bar{\omega}} \\ \Delta A_{\langle-\omega\partial q/\partial p\rangle;A_{\omega}} \\ \Delta A_{\langle-\omega\partial q/\partial p\rangle;\phi_{\omega}} \\ \Delta A_{\langle-\omega\partial q/\partial p\rangle;\partial\bar{q}/\partial p} \\ \Delta A_{\langle-\omega\partial q/\partial p\rangle;A_{\partial q/\partial p}} \\ \Delta A_{\langle-\omega\partial q/\partial p\rangle;\phi_{\partial q/\partial p}} \end{bmatrix} = \begin{bmatrix} \cos(\phi_{\langle-\omega\partial q/\partial p\rangle} - \phi_{\langle-\Delta\bar{\omega}\partial\{q'\}/\partial p\rangle})\Delta A_{\langle-\Delta\bar{\omega}\partial\{q'\}/\partial p\rangle} + A_{\langle-\Delta\bar{\omega}\partial\{q'\}/\partial p\rangle} \\ \sin(\phi_{\langle-\omega\partial q/\partial p\rangle} - \phi_{\langle-\Delta\bar{\omega}\partial\{q'\}/\partial p\rangle})\Delta\phi_{\langle-\Delta\bar{\omega}\partial\{q'\}/\partial p\rangle} \\ \cos(\phi_{\langle-\omega\partial q/\partial p\rangle} - \phi_{\langle-\{\Delta\omega'\}\partial\bar{q}/\partial p\rangle})\Delta A_{\langle-\{\Delta\omega'\}\partial\bar{q}/\partial p\rangle;\Delta A_{\omega}} + A_{\langle-\{\Delta\omega'\}\partial\bar{q}/\partial p\rangle} \\ \sin(\phi_{\langle-\omega\partial q/\partial p\rangle} - \phi_{\langle-\{\Delta\omega'\}\partial\bar{q}/\partial p\rangle})\Delta\phi_{\langle-\{\Delta\omega'\}\partial\bar{q}/\partial p\rangle;\Delta A_{\omega}} \\ \cos(\phi_{\langle-\omega\partial q/\partial p\rangle} - \phi_{\langle-\{\Delta\omega'\}\partial\bar{q}/\partial p\rangle})\Delta A_{\langle-\{\Delta\omega'\}\partial\bar{q}/\partial p\rangle;\Delta\phi_{\omega}} + A_{\langle-\{\Delta\omega'\}\partial\bar{q}/\partial p\rangle} \\ \sin(\phi_{\langle-\omega\partial q/\partial p\rangle} - \phi_{\langle-\{\Delta\omega'\}\partial\bar{q}/\partial p\rangle})\Delta\phi_{\langle-\{\Delta\omega'\}\partial\bar{q}/\partial p\rangle;\Delta\phi_{\omega}} \\ \cos(\phi_{\langle-\omega\partial q/\partial p\rangle} - \phi_{\langle-\{\omega'\}\partial\Delta\bar{q}/\partial p\rangle})\Delta A_{\langle-\{\omega'\}\partial\Delta\bar{q}/\partial p\rangle} + A_{\langle-\{\omega'\}\partial\Delta\bar{q}/\partial p\rangle} \\ \sin(\phi_{\langle-\omega\partial q/\partial p\rangle} - \phi_{\langle-\{\omega'\}\partial\Delta\bar{q}/\partial p\rangle})\Delta\phi_{\langle-\{\omega'\}\partial\Delta\bar{q}/\partial p\rangle} \\ \cos(\phi_{\langle-\omega\partial q/\partial p\rangle} - \phi_{\langle-\bar{\omega}\partial\{\Delta q'\}/\partial p\rangle})\Delta A_{\langle-\bar{\omega}\partial\{\Delta q'\}/\partial p\rangle;\Delta A_q} + A_{\langle-\bar{\omega}\partial\{\Delta q'\}/\partial p\rangle} \\ \sin(\phi_{\langle-\omega\partial q/\partial p\rangle} - \phi_{\langle-\bar{\omega}\partial\{\Delta q'\}/\partial p\rangle})\Delta\phi_{\langle-\bar{\omega}\partial\{\Delta q'\}/\partial p\rangle;\Delta A_q} \\ \cos(\phi_{\langle-\omega\partial q/\partial p\rangle} - \phi_{\langle-\bar{\omega}\partial\{\Delta q'\}/\partial p\rangle})\Delta A_{\langle-\bar{\omega}\partial\{\Delta q'\}/\partial p\rangle;\Delta\phi_q} + A_{\langle-\bar{\omega}\partial\{\Delta q'\}/\partial p\rangle} \\ \sin(\phi_{\langle-\omega\partial q/\partial p\rangle} - \phi_{\langle-\bar{\omega}\partial\{\Delta q'\}/\partial p\rangle})\Delta\phi_{\langle-\bar{\omega}\partial\{\Delta q'\}/\partial p\rangle;\Delta\phi_q} \end{bmatrix} \quad (B11)$$

$$\begin{bmatrix} \Delta\phi_{(-\omega\partial q/\partial p);\bar{\omega}} \\ \Delta\phi_{(-\omega\partial q/\partial p);A_\omega} \\ \Delta\phi_{(-\omega\partial q/\partial p);\phi_\omega} \\ \Delta\phi_{(-\omega\partial q/\partial p);\partial\bar{q}/\partial p} \\ \Delta\phi_{(-\omega\partial q/\partial p);A_{\partial q/\partial p}} \\ \Delta\phi_{(-\omega\partial q/\partial p);\phi_{\partial q/\partial p}} \end{bmatrix} = \frac{1}{A_{(-\omega\partial q/\partial p)}} \times \begin{bmatrix} \sin(\phi_{(-\Delta\bar{\omega}\{q'\}/\partial p)} - \phi_{(-\omega\partial q/\partial p)})\Delta A_{(-\Delta\bar{\omega}\{q'\}/\partial p)} + A_{(-\Delta\bar{\omega}\{q'\}/\partial p)} \\ \cos(\phi_{(-\Delta\bar{\omega}\{q'\}/\partial p)} - \phi_{(-\omega\partial q/\partial p)})\Delta\phi_{(-\Delta\bar{\omega}\{q'\}/\partial p)} \\ \sin(\phi_{(-\{\Delta\omega'\}\partial\bar{q}/\partial p)} - \phi_{(-\omega\partial q/\partial p)})\Delta A_{(-\{\Delta\omega'\}\partial\bar{q}/\partial p);A_\omega} + A_{(-\{\Delta\omega'\}\partial\bar{q}/\partial p)} \\ \cos(\phi_{(-\{\Delta\omega'\}\partial\bar{q}/\partial p)} - \phi_{(-\omega\partial q/\partial p)})\Delta\phi_{(-\{\Delta\omega'\}\partial\bar{q}/\partial p);A_\omega} \\ \sin(\phi_{(-\{\Delta\omega'\}\partial\bar{q}/\partial p)} - \phi_{(-\omega\partial q/\partial p)})\Delta A_{(-\{\Delta\omega'\}\partial\bar{q}/\partial p);\Delta\phi_\omega} + A_{(-\{\Delta\omega'\}\partial\bar{q}/\partial p)} \\ \cos(\phi_{(-\{\Delta\omega'\}\partial\bar{q}/\partial p)} - \phi_{(-\omega\partial q/\partial p)})\Delta\phi_{(-\{\Delta\omega'\}\partial\bar{q}/\partial p);\Delta\phi_\omega} \\ \sin(\phi_{(-\{\omega'\}\partial\Delta\bar{q}/\partial p)} - \phi_{(-\omega\partial q/\partial p)})\Delta A_{(-\{\omega'\}\partial\Delta\bar{q}/\partial p)} + A_{(-\{\omega'\}\partial\Delta\bar{q}/\partial p)} \\ \cos(\phi_{(-\{\omega'\}\partial\Delta\bar{q}/\partial p)} - \phi_{(-\omega\partial q/\partial p)})\Delta\phi_{(-\{\omega'\}\partial\Delta\bar{q}/\partial p)} \\ \sin(\phi_{(-\bar{\omega}\partial\{\Delta q'\}/\partial p)} - \phi_{(-\omega\partial q/\partial p)})\Delta A_{(-\bar{\omega}\partial\{\Delta q'\}/\partial p);A_q} + A_{(-\bar{\omega}\partial\{\Delta q'\}/\partial p)} \\ \cos(\phi_{(-\bar{\omega}\partial\{\Delta q'\}/\partial p)} - \phi_{(-\omega\partial q/\partial p)})\Delta\phi_{(-\bar{\omega}\partial\{\Delta q'\}/\partial p);A_q} \\ \sin(\phi_{(-\bar{\omega}\partial\{\Delta q'\}/\partial p)} - \phi_{(-\omega\partial q/\partial p)})\Delta A_{(-\bar{\omega}\partial\{\Delta q'\}/\partial p);\Delta\phi_q} + A_{(-\bar{\omega}\partial\{\Delta q'\}/\partial p)} \\ \cos(\phi_{(-\bar{\omega}\partial\{\Delta q'\}/\partial p)} - \phi_{(-\omega\partial q/\partial p)})\Delta\phi_{(-\bar{\omega}\partial\{\Delta q'\}/\partial p);\Delta\phi_q} \end{bmatrix} \quad (\text{B12})$$

## REFERENCES

- Biasutti, M., 2013: Forced Sahel rainfall trends in the CMIP5 archive. *J. Geophys. Res.*, **118**, 1613–1623, doi:10.1002/jgrd.50206.
- , and A. Sobel, 2009: Delayed Sahel rainfall and global seasonal cycle in a warmer climate. *Geophys. Res. Lett.*, **36**, L23707, doi:10.1029/2009GL041303.
- , D. S. Battisti, and E. S. Sarachik, 2003: The annual cycle over the tropical Atlantic, South America, and Africa. *J. Climate*, **16**, 2491–2508, doi:10.1175/1520-0442(2003)016<2491:TACOTT>2.0.CO;2.
- , —, and —, 2004: Mechanisms controlling the annual cycle of precipitation in the tropical Atlantic sector in an atmospheric GCM. *J. Climate*, **17**, 4708–4723, doi:10.1175/JCLI-3235.1.
- Cess, R. D., and Coauthors, 1990: Intercomparison and interpretation of climate feedback processes in 19 atmospheric general circulation models. *J. Geophys. Res.*, **95**, 16 601–16 615, doi:10.1029/JD095iD10p16601.
- Chiang, J. C. H., and A. H. Sobel, 2002: Tropical tropospheric temperature variations caused by ENSO and their influence on the remote tropical climate. *J. Climate*, **15**, 2616–2631, doi:10.1175/1520-0442(2002)015<2616:TTVCB>2.0.CO;2.
- Chou, C., and J. D. Neelin, 2004: Mechanisms of global warming impacts on regional tropical precipitation. *J. Climate*, **17**, 2688–2701, doi:10.1175/1520-0442(2004)017<2688:MOGWIO>2.0.CO;2.
- , and C.-W. Lan, 2012: Changes in the annual range of precipitation under global warming. *J. Climate*, **25**, 222–235, doi:10.1175/JCLI-D-11-00097.1.
- , J.-Y. Tu, and P.-H. Tan, 2007: Asymmetry of tropical precipitation change under global warming. *Geophys. Res. Lett.*, **34**, L17708, doi:10.1029/2007GL030327.
- Dwyer, J. G., M. Biasutti, and A. H. Sobel, 2012: Projected changes in the seasonal cycle of surface temperature. *J. Climate*, **25**, 6359–6374, doi:10.1175/JCLI-D-11-00741.1.
- Emanuel, K., and A. Sobel, 2013: Response of tropical sea surface temperature, precipitation, and tropical cyclone-related variables to changes in global and local forcing. *J. Adv. Model. Earth Syst.*, **5**, 447–458, doi:10.1002/jame.20032.
- Fu, R., R. E. Dickinson, M. Chen, and H. Wang, 2001: How do tropical sea surface temperatures influence the seasonal distribution of precipitation in the equatorial Amazon? *J. Climate*, **14**, 4003–4026, doi:10.1175/1520-0442(2001)014<4003:HDTSSST>2.0.CO;2.
- Fu, X., and B. Wang, 2004: Differences of boreal summer intraseasonal oscillations simulated in an atmosphere–ocean coupled model and an atmosphere-only model. *J. Climate*, **17**, 1263–1271, doi:10.1175/1520-0442(2004)017<1263:DOBSIO>2.0.CO;2.
- Gent, P. R., and Coauthors, 2011: The Community Climate System Model version 4. *J. Climate*, **24**, 4973–4991, doi:10.1175/2011JCLI4083.1.
- Held, I., and B. Soden, 2006: Robust responses of the hydrological cycle to global warming. *J. Climate*, **19**, 5686–5699, doi:10.1175/JCLI3990.1.
- Huang, P., S.-P. Xie, K. Hu, G. Huang, and R. Huang, 2013: Patterns of the seasonal response of tropical rainfall to global warming. *Nat. Geosci.*, **6**, 357–361, doi:10.1038/ngeo1792.
- Hurrell, J. W., J. J. Hack, D. Shea, J. M. Caron, and J. Rosinski, 2008: A new sea surface temperature and sea ice boundary dataset for the Community Atmosphere Model. *J. Climate*, **21**, 5145–5153, doi:10.1175/2008JCLI2292.1.
- Kitoh, A., and O. Arakawa, 1999: On overestimation of tropical precipitation by an atmospheric GCM with prescribed SST. *Geophys. Res. Lett.*, **26**, 2965–2968, doi:10.1029/1999GL900616.
- Kutzbach, J., 1967: Empirical eigenvectors of sea-level pressure, surface temperature and precipitation complexes over North America. *J. Appl. Meteor.*, **6**, 791–802, doi:10.1175/1520-0450(1967)006<0791:EEOSLP>2.0.CO;2.
- Li, T., and S. G. H. Philander, 1997: On the seasonal cycle of the equatorial Atlantic Ocean. *J. Climate*, **10**, 813–817, doi:10.1175/1520-0442(1997)010<0813:OTSCOT>2.0.CO;2.
- Lin, J.-L., 2007: The double-ITCZ problem in IPCC AR4 coupled GCMs: Ocean–atmosphere feedback analysis. *J. Climate*, **20**, 4497–4525, doi:10.1175/JCLI4272.1.
- Liu, C., R. P. Allan, and G. J. Huffman, 2012: Co-variation of temperature and precipitation in CMIP5 models and satellite

- observations. *Geophys. Res. Lett.*, **39**, L13803, doi:10.1029/2012GL052093.
- Meehl, G. A., C. Covey, K. E. Taylor, T. Delworth, R. J. Stouffer, M. Latif, B. McAvaney, and J. F. B. Mitchell, 2007: The WCRP CMIP3 multimodel dataset: A new era in climate change research. *Bull. Amer. Meteor. Soc.*, **88**, 1383–1394, doi:10.1175/BAMS-88-9-1383.
- Seager, R., and N. Henderson, 2013: Diagnostic computation of moisture budgets in the ERA-Interim reanalysis with reference to analysis of CMIP-archived atmospheric model data. *J. Climate*, **26**, 7876–7901, doi:10.1175/JCLI-D-13-00018.1.
- Seth, A., S. A. Rauscher, M. Rojas, A. Giannini, and S. J. Camargo, 2011: Enhanced spring convective barrier for monsoons in a warmer world? *Climatic Change*, **104**, 403–414, doi:10.1007/s10584-010-9973-8.
- , —, M. Biasutti, A. Giannini, S. J. Camargo, and M. Rojas, 2013: CMIP5 projected changes in the annual cycle of precipitation in monsoon regions. *J. Climate*, **26**, 7328–7351, doi:10.1175/JCLI-D-12-00726.1.
- Shukla, J., and M. Fennessy, 1994: Simulation and predictability of monsoons. Proceedings of the International Conference on Monsoon Variability and Prediction, World Climate Research Program Tech. Rep. WCRP-84, 567–575.
- Sobel, A., and S. Camargo, 2011: Projected future seasonal changes in tropical summer climate. *J. Climate*, **24**, 473–487, doi:10.1175/2010JCLI3748.1.
- Tan, P.-H., C. Chou, and J.-Y. Tu, 2008: Mechanisms of global warming impacts on robustness of tropical precipitation asymmetry. *J. Climate*, **21**, 5585–5602, doi:10.1175/2008JCLI2154.1.
- Taylor, K. E., R. J. Stouffer, and G. A. Meehl, 2012: An overview of CMIP5 and the experiment design. *Bull. Amer. Meteor. Soc.*, **93**, 485–498, doi:10.1175/BAMS-D-11-00094.1.
- Vecchi, G. A., B. J. Soden, A. T. Wittenberg, I. M. Held, A. Leetmaa, and M. J. Harrison, 2006: Weakening of tropical Pacific atmospheric circulation due to anthropogenic forcing. *Nature*, **441**, 73–76, doi:10.1038/nature04744.
- Wu, R., and B. Kirtman, 2005: Roles of Indian and Pacific Ocean air–sea coupling in tropical atmospheric variability. *Climate Dyn.*, **25**, 155–170, doi:10.1007/s00382-005-0003-x.
- , and —, 2007: Regimes of seasonal air–sea interaction and implications for performance of forced simulations. *Climate Dyn.*, **29**, 393–410, doi:10.1007/s00382-007-0246-9.
- Xie, S.-P., C. Deser, G. A. Vecchi, J. Ma, H. Teng, and A. T. Wittenberg, 2010: Global warming pattern formation: Sea surface temperature and rainfall. *J. Climate*, **23**, 966–986, doi:10.1175/2009JCLI3329.1.